Applied Ocean Research 166 (2026) 104925

Contents lists available at ScienceDirect

Applied Ocean Research

journal homepage: www.elsevier.com/locate/apor

Research paper

Designing robust adaptive ensemble deep learning based decomposition technique for sea level variability prediction

Mohammed Diykh [a,b,f], Mumtaz Ali [b,*], Aitazaz Ahsan Farooque [a,e], Anwar Ali Aldhafeeri [c,*], Abdulhaleem H. Labban [d]

[a] Canadian Centre for Climate Change and Adaptation, University of Prince Edward Island, St Peter's Bay, PE, Canada
[b] School of Business, Law, Humanities, and Pathways, University of Southern Queensland, QLD 4305, Australia
[c] Department of Mathematics and Statistics, Faculty of Science, King Faisal University, P.O. Box 400, Al-Ahsa, 31982, Saudi Arabia
[d] Department of Meteorology, Faculty of Environmental Sciences, King Abdulaziz University, Jeddah 21589, Saudi Arabia
[e] Faculty of Sustainable Design Engineering, University of Prince Edward Island, Charlottetown, PE, Canada
[f] Engineering Technical College, Al-Ayen Iraqi University, Thi-Qar, Nasiriyah, 64001, Iraq

ARTICLE INFO

Keywords:
Sea level variability
CEEMDAN
Graph
Ensemble
HFS
OLSSA

ABSTRACT

Sea level variability is an urgent climate risk, threatening to vanish islands and coastal areas. Forecasting future sea level rise accurately is fundamental to support experts for flooding and erosion control. In this paper, a novel sea level variability forecast model (CG-CEEMDAN—HFS-AEM) is proposed integrating correlation graph (CG), a complete ensemble empirical mode decomposition with adaptive noise (CEEMDAN), Hilbert feature selection approach (HFS), adaptive ensemble model (AEM), and oppositional learning sparrow search algorithm (OLSSA). The AEM is a novel ensemble model that combines the strengths of GRU, self-attention LSTM and XGBoost models based on dynamic weights assignment strategy, adjusting to real-time changes in sea level rise by updating the weights according to the error and performance of the models. Firstly, the input data is pre-processed using correlation graph to remove lower correlated variables and fill the missing values in the data. After that the CEEMDAN technique is employed to decompose the data, followed by HFS to select the most efficient features. The selected features are then employed into the AEM model where the OLSSA is adopted to select the optimal hyper-parameters of the proposed model. To verify the efficiency of the proposed CG-CEEMDAN—HFS-AEM against comparing models, extensive experiments were conducted to forecast sea level variability for Hillary and Burnie stations in Australia. The results shows that the proposed model obtained the highest accuracy in terms of goodness-of-fit metrics against the state-of-the-art benchmark comparing models. The proposed model can offer a valuable tool for coastal planning and policy making under the recent climate change.

1. Introduction

Sea level rise is considered a major global environmental problem and requires and urgent solutions in the rising climate change. Understanding the mechanisms, and behaviour of sea level rise is essential for evaluating its impacts on coastal areas and ecosystems. Coastal systems produce non-linear and complex data (Makarynska and Makarynskyy, 2008; Ghorbani et al., 2010) and understanding the behaviour and interaction process of coastal systems is vital in preventing erosion which is a natural process increased by human activity and climate changes (Pashova and Popova, 2011; Karimi, Kisi et al., 2013; Imani, Kao et al., 2018; Lai, Ahmed et al., 2019). Designing accurate model to monitor sea level rise can improve development risk management strategies and minimise global environmental issues. Recent studies showed that sea level rise is highly influenced by changes associated with waves, wind patterns, and coastal circulation leading to increase the risk of flooding and erosion (Li, Zhou et al., 2025).

Recent several statistical based approaches such as Gaussian Process Regression (GPR), SARIMA, and linear trend based autoregressive (Aksoy, Mowla et al., 2025; Givehki, Melby et al., 2025) have been widely employed for sea level prediction, however, these techniques are primarily suitable for stationary or near linear time series.

* Corresponding authors.
E-mail addresses: mumtaz.ali@unisq.edu.au (M. Ali), aaldhafeeri@kfu.edu.sa (A.A. Aldhafeeri).

https://doi.org/10.1016/j.apor.2026.104925
Received 18 September 2025; Received in revised form 2 January 2026; Accepted 5 January 2026
Available online 10 January 2026

Correspondingly, semi empirical temperature sea level relationships have been developed for long term climate sea level rise rather than short term variability. In contrast, the tide gauge data used in this study exhibited strong non stationarity, and nonlinear relationships driven by tides, meteorological forcing, and coastal dynamics. These patterns limit the performance of simple statistical or trend-based approaches. Therefore, in this paper, a robust model is designed which integrates CEEMDAN, Hilbert features, graph correlation, and deep learning models to better capture the nonlinear and multi scale patterns of short-term sea-level fluctuations.

Meteorological data and sea level measurements are used to monitor and predict sea level variation at coastal areas. For example, Tide gauges are employed to monitor sea level in terms of low and high-frequency based one different meteorological factor including pressure, air temperature, and humidity (Kowalewski and Kowalewska-Kalkowska, 2017; Parker and Ollier, 2017; Liang, Hu et al., 2023). Literature shows that the harmonic analysis techniques is considered to predict sea level rise, but it required long, continuous data analyse along with inability to fully capture nonlinearities (El-Diasty, Al-Harbi et al., 2018; Hsieh, Chou et al., 2022; Zhang, Cui et al., 2025). Due to this issue, harmonic techniques could produce huge errors as long-term sea level data are essential for accurate prediction. As a result, machine learning (ML) models can predict accurately (Imani, Kao et al., 2018; Zhao, Cai et al., 2021; Alshouny, Elnabwy et al., 2022; Xu, Matsushima et al., 2024; Li, Zhou et al., 2025; Majumder, Abeer et al., 2025).

Recently, several machine learning-based approaches have been designed to predict long-term and short-term sea-level rise using air pressure, air temperature, humidity. Wang et al. (2025) designed UNet based temporal spatial Transformer Attention model for sea level anomaly prediction. Their model was tested on dataset collected from Altimeter satellite gridded Sea Level Anomalies. Latif et al. (2024) examined the ability of k-Nearest Neighbours (kNN) and Support Vector Machine (SVM) models for sea level prediction. XU et al. (2024) studies the impacts of sea level rise in Japan. They conducted geo-detector analysis, field surveys, and coastal inundation approaches in that study. Makarynska and Makarynskyy (2008) utilised an artificial neural network (ANN) to assess sea level in Australia. Majumder, Abeer et al. (2025) investigated the ability of empirical orthogonal functions coupled with dynamic mode decomposition to predict sea level rise along the US East and Gulf coasts and its socio-economic impacts on the nearby inland areas while Latif, Almubaidin et al. (2024) combined k-nearest neighbour with support vector machine (SVM) and showed that SVM is better than comparing models. A sea level prediction model based on ANN with decomposition technique was proposed by Pashova and Popova (2011) using historical data to predict 12, 24, 36, 48, and 60 h ahead. Genetic programming (GP) and ANN models were employed to predict seal level in Australia using the data from 1992–2002 (Ghorbani, Khatibi et al., 2010). Pashova and Popova (2011) applied multilayer Feed-Forward, Cascade-Feed-Forward, Feed-Forward Time-Delay, Radial Basis Function, Generalized Regression neural networks and Multiple Linear regression and ANN models for daily sea level forecast at tide gauge in Burgas, Bulgaria. Karimi, Kisi et al. (2013) examined different machine learning model including Neuro-fuzzy and neural network techniques for forecasting sea level in Darwin Harbor, Australia and showed that Neuro-fuzzy recorded the highest accuracy. Imani, Kao et al. (2018) applied extreme learning machine (ELM) to time series data for the period 2004–2011 from Dongshi tide gauge station in Taiwan to predict sea level. Altunkaynak and Kartal (Altunkaynak and Kartal, 2021) combined wavelet transforms with fuzzy logic to forecast sea level for four stations in Bosporus. Li, Zhou et al. (2025) applied CNN-BiGRU for sea level height prediction combined with Bayesian optimization algorithm.

Although the mentioned methods in the above literature have made contributions where most of those sea level prediction models have considered only one or two variables; however, actual sea level variability is affected by multiple oceanic drivers and measures. Moreover, most of these studies applied classical machine learning models which often requires significant feature engineering, struggling with complex, non-linear relationships, and may not generalize well to unseen data. In this research an intelligent model CG-CEEMDAN—HFS-AEM is designed to forecast sea level for Burnie and Hillarys stations in Australia. The novelty of this work did not lie in reintroducing these techniques independently, but rather in their unified integration into a coherent, adaptive prediction architecture specifically tailored for non-stationary sea level variability. This study proposes, for the first time, a Correlation Graph guided decomposition model (CG-CEEMDAN) combined with a Hilbert-based feature selection mechanism (HFS) that filters IMFs according to temporal relevance rather than using decomposition outputs blindly. Additionally, the Adaptive Ensemble Model (AEM) suggests a dynamic weight updating scheme that continuously recalibrates GRU, self-attention LSTM, and XGBoost contributions based on instantaneous error trends, enabling the proposed model to respond to sudden sea level fluctuations. The integration of OLSSA further enhances this adaptiveness by optimising model specific hyperparameters at each stage. This designed model employed specifically for multi scale ocean variability prediction, differs fundamentally from prior works that apply these techniques in isolation.

In this paper, predicting sea level variability is adopted, because most prediction error in real world coastal hazards happened from non-tidal drivers, comparing the proposed hybrid CG-CEEMDAN—HFS-AEM model with harmonic analysis would not establish an equitable or scientifically meaningful comparison.

The CG-CEEMDAN—HFS-AEM model includes four phases. Phase 1 identifies the optimal variables set using the correlation graph (CG) method. The CG received the input multivariant time series and determine the most effective variables. In phase 2, a complete ensemble empirical mode decomposition with adaptive noise (CEEMDAN), and Hilbert feature selection approach (HFS) are utilised to decompose sea level time series and select the most effective and significant features. The number of modes is selected empirically based on the HFS. Phase 3 designing the main prediction model adaptive ensemble model (AEM) which is applied for each mode separately. The AEM is a novel ensemble model that combines the strengths of GRU, self-attention LSTM and XGBoost models based on dynamic weights assignment strategy, adjusting to real-time changes in sea level rise by updating the weights according to the error and performance of the models while phase 4 adopted oppositional learning sparrow search algorithm (OLSSA) to select the most optimal the hyper-parameters of AEM. The AEM model learns to adapt by modifying the individual models it uses, their weights, or even replacing them with better performing ones over time to improve prediction accuracy and robustness.

2. Data description

Globally, Australia is a largest island-continent with a diverse coasts and shorelines. The rise of sea level in Australia created several significant challenges to coastlines. These challenges need pre-emptive adaptation actions and strategies to tackle the sea level rise. The sea level rise is anticipated to drastically impact coastal communities, infrastructure, and ecosystems due to intensified flooding, erosion, and storm surges. The impact will be so sever influencing from beaches and coral reefs to transportation networks and residential areas. In this study, the sea level data were acquired from the Bureau of Meteorology (BoM), Australia for Hillarys station in the state of Western Australia and Burnie station from Tasmania state. The time interval of the data is hourly from 01/01/1999 to 31/03/2024 recorded by a Sea level Fine Resolution Acoustic Measuring Equipment station under the Baseline Sea Level Monitoring Project. Hillarys station is the main harbour in the north metropolitan zone of Perth city and is a place for holding ships and boats. The Burnie station in Tasmania, Australia, is also involved in the Baseline Sea Level Monitoring Project to examine sea level variations. This station is positioned at the seaport of Burnie in northern Tasmania.

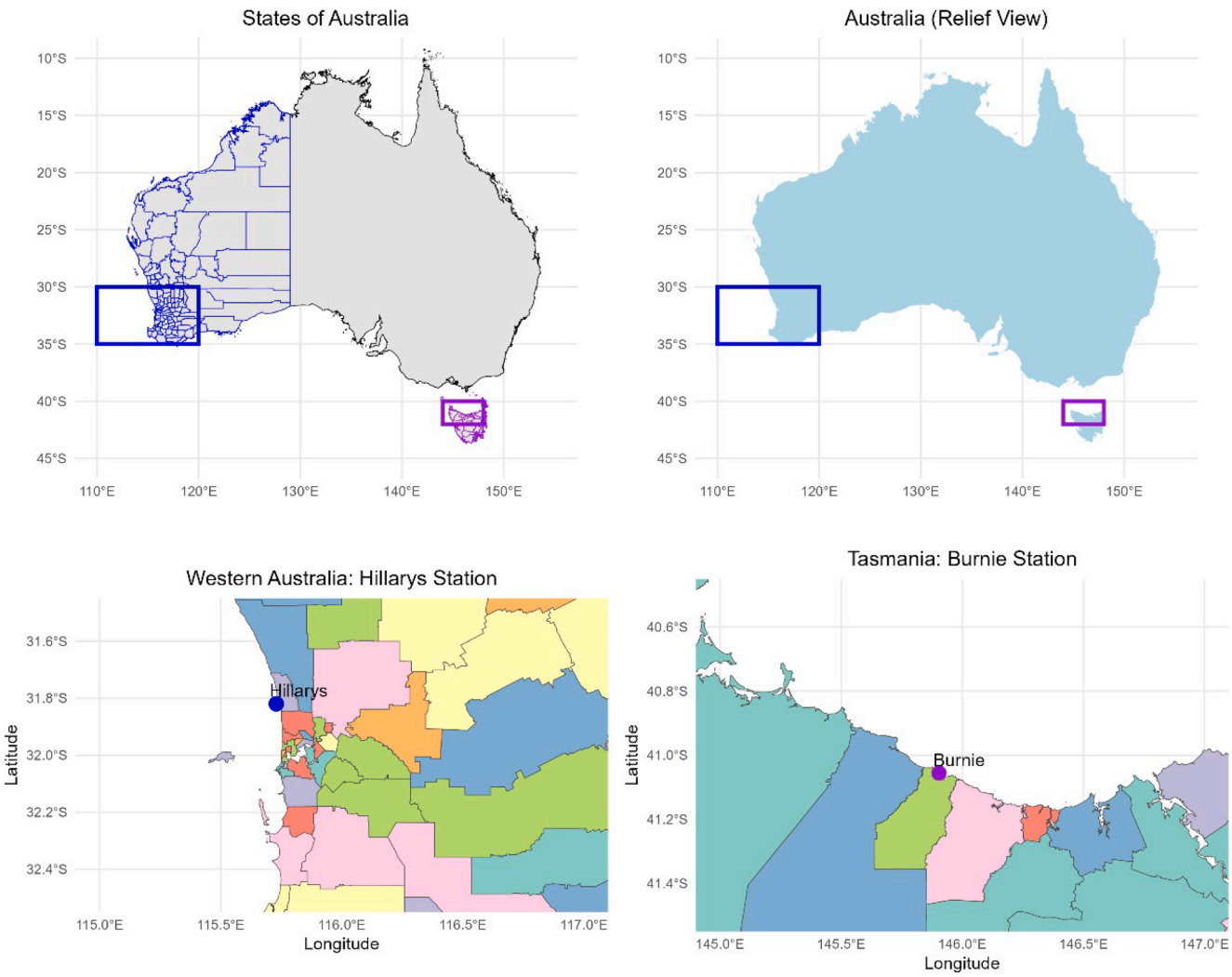

Fig. 1. Map of the stations.

The station of Burnie tide gauge was utilized to re-establish heights on the Australian Height Datum (Tasmania) in 1983. The data include water temperature, air temperature, Barometric pressure, residuals, adjusted residuals, wind direction, wind gust, wind speed as the input variables and sea level as the target or objective variable. The sea levels are in recorded in metres above Tide Gauge Zero. The water and air temperatures are measured in degrees Celsius whereas the Barometric Pressures are in hPa. The residual and adjusted residuals are calculated in metres and the wind directions in degrees True which is the average of the last six, one-minute wind direction measurements taken in the previous hour. The input variables wind gust and wind speed are in are measured in m/*sec*. The wind gust is the maximum of the sixty, one-minute wind gust measurements while the wind speed is the mean of the last six, one-minute measurements recorded in the previous hour. The data also contains missing values which were replaced with the mean value of the corresponding variable. A map of these stations is supplied in Fig. 1 and Fig. 2 shows the time-series trends plot of data variables.

3. Methods

3.1. Correlation graph (CG)

A graph correlation provides a powerful methodology to analysis multivariate time series data and its variables relationships (Mittal, Sachdeva et al., 2021). The proposed correlation graph model exposes complex relationship and dynamic interactions between diverse time-dependent variables (Pedronette and Torres, 2016). By employing correlation networks, in this paper, the sea level time series is effectively visualized and analysed to find the strength and direction of relationships among the variables (Qi, Lin et al., 2022).

3.2. Complete ensemble empirical mode decomposition (CEEMDAN)

CEEMDAN is a powerful decomposition model which has been designed to decompose non-stationary and non-linear time data into intrinsic mode functions (IMFs) with adaptive noise assistance (Du, Xia et al., 2021). It's an advanced version of ensemble empirical mode decomposition (EEMD), and empirical mode decomposition (EMD) (Zeiler, Faltermeier et al., 2010; Xiao, Wu et al., 2024).

Suppose a time-series $X = \{X_1(t), X_2(t), \ldots, X_p(t)\}$, using CEEMDAN technique the time series data X is decomposed it into multiple intrinsic mode functions (IMFs) while minimising mode mixing through adding adaptive Gaussian white noise. The main procedures of the CEEMDAN are as follows:

- **Phase 1:** In this stage, Gaussian white noise is added to the original data, suppose X is the original sequence, then using Eq. (1) then Gaussian white noise φ is added with signal-to-noise ratio ε as shown in Eq. (1).

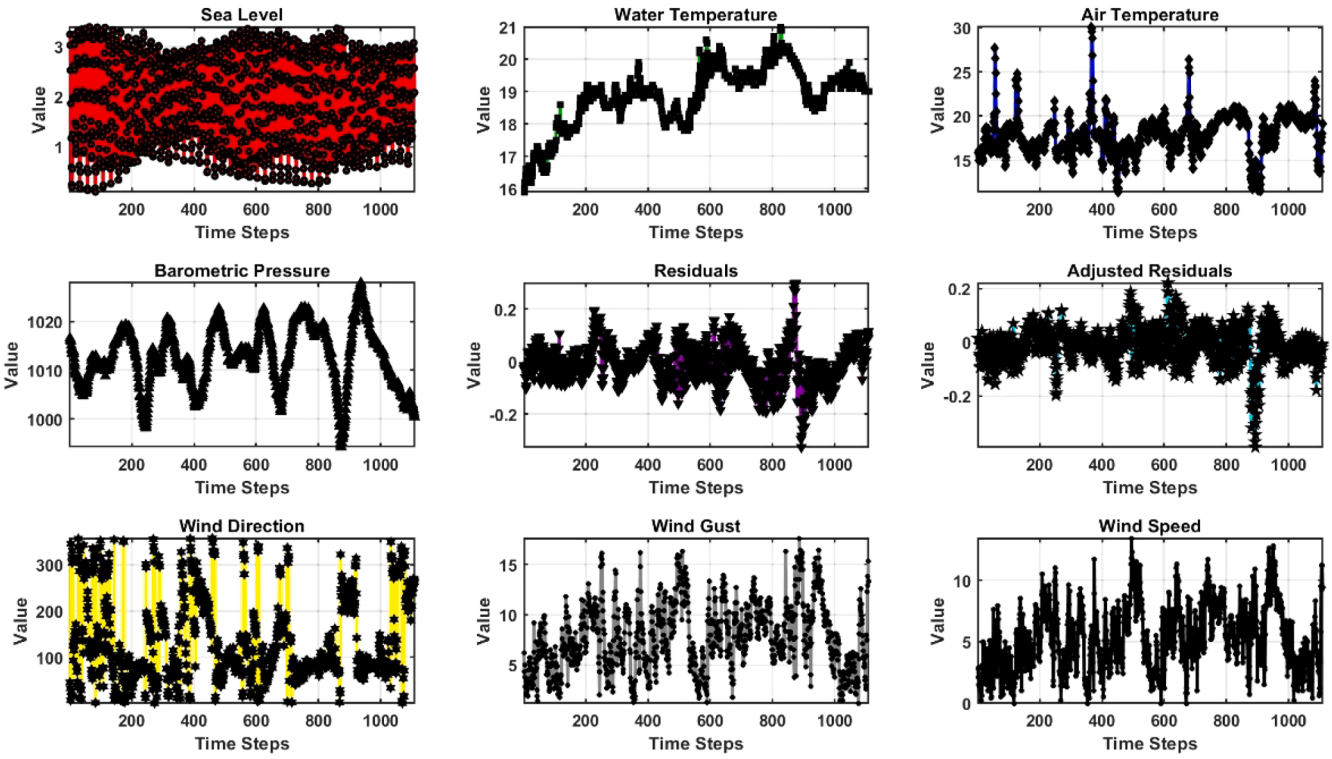

Fig. 2. Time-series trends plot of data variables.

$$X_i = X + \varepsilon\varphi_i \tag{1}$$

after that EMD is applied to attain the residual and first intrinsic mode function (IMF) as shown in Eq. (2).

$$EMD(X_i) = imf_i + res_i \tag{2}$$

Where imf_i denotes to the first IMF obtained from the noisy sequence, $\varepsilon\varphi_i$ refers to the remaining residual.

- **Phase 2**: In this stage, the first-order IMF of CEEMDAN is computed from averaging all IMFs acquired through different noise realizations as shown in Eq. (5)

$$IMF_1 = \frac{1}{I}\sum_{i=1}^{I} imf_{i1} \tag{3}$$

Where IMF_1 is the first-order IMF. Then, the first-order residual r_1 is calculated by subtracting IMF_1 from X as shown in Eq. (4).

$$r_1 = X - IMF_1 \tag{4}$$

- **Phase 3**: In this stage, the EMD applied on Gaussian white noise φ to calculate its Second-Order IMF $E_1(\varphi)$. Firstly, r_1 is updated by adding $E_1(\varphi)$ as shown in Eq. (7)

$$r_1 + \varepsilon E_1(\varphi) \tag{5}$$

Then, the EMD is applied again to achieve the second-order IMF as shown in Eq. (8)

$$IMF_2 = \frac{1}{I}\sum_{i=1}^{I} E_1(r_1 + \varepsilon E_1(\varphi)) \tag{6}$$

Finally, the second-order residual r_2 is calculated as shown in Eq. (9)

$$r_2 = r_1 - IMF_2 \tag{7}$$

- **Phase 4**: In this stage, all procedures in phases 1,2, and 3 are repeated until the residual amplitude drops below a predefined threshold using Eq. (10)

$$IMF_k = \frac{1}{I}\sum_{i=1}^{I} E_1(r_{k-1} + \varepsilon E_{k-1}(\varphi_i)) \tag{8}$$

Where IMF_k denotes to the k-th mode obtained from residual.

- **Phase 5**: In this phase, the final residual component is calculated after all IMF_k are extracted using Eq. (9).

$$R = Y - \sum_{k=1}^{K} IMF_k \tag{9}$$

3.3. Hilbert feature selection approach (HFS)

CEEMDAN decomposes the time series into multiple Intrinsic Mode Functions (IMFs). The feature selection HFS model is designed to determine which IMFs contain meaningful predictive information and which ones produce noise, redundancy, or spurious oscillations. The HFS module was employed to prevent model degradation caused by irrelevant or highly correlated IMFs, and to reduce computational

complexity by selecting only the most informative components.

Suppose a time series is divided into multiple Intrinsic Mode Functions

$$IMFs = \{ IMF_1, IMF_2, \ldots. IMF_n\} \tag{10}$$

Then each IMF_i is segmented inti blocks

$$IMF_i = \{ block_1, block_2, \ldots block_m\} \tag{11}$$

The similarity between each pair of blocks HS ($Block_i$, $Block_j$) is calculated using the following formula.

$$Similarity\ (x,y) = \frac{\sum_{i=1}^{n}(Block_i * Block_i) - \max\ (Block_i)}{||Block_i|| * ||Block_j||} \tag{12}$$

Where

$$Block_i = \sqrt{X_1^2 + x_2^2 + x_3^2 + \ldots. + x_n^2} \tag{13}$$

$$Block_j = \sqrt{y_1^2 + y_2^2 + y_3^2 + \ldots. + y_n^2} \tag{14}$$

The proposed HFS model relies on the Hilbert similarity index, which quantifies the intrinsic similarity structure of each IMF by analysing its local oscillatory behaviour across time segments. Each IMF is divided into multiple blocks, and the Hilbert convex similarity was computed between blocks to measure the internal consistency of the IMF. IMFs exhibiting high Hilbert similarity show stable, coherent temporal patterns and therefore carry meaningful physical information about long or short-term sea level behaviour, while low similarity IMFs represent noise or irregular oscillations.

The proposed Hilbert model serves as a numerical relevance score that ranks IMFs based on temporal coherence. Only IMFs exceeding a predefined similarity threshold are retained and forwarded to the ensemble model. Through this mechanism, HFS works as a data-driven filter that automatically removes unstable or redundant IMFs before prediction. This not only enhances the model's interpretability but also stabilises training and improves forecasting accuracy by ensuring that the ensemble learns from the most physically meaningful features extracted from CEEMDAN.

3.4. Extreme gradient boosting (XGBoost)

The XGBoost (Chen, He et al., 2015) is an ensemble perdition model that integrates the predictive results of several weak models to generate a stronger prediction. Due to its ability to process large time series data and achieves high prediction rate, it becomes one of the most popular machine learning approach (Ali, Abduljabbar et al., 2023). XGBoost is suitable for nonstationary and irregular dataset such as sea level prediction as its able to capture the hidden and complex relationships among sea level prediction variables, Sea Level, Water Temperature, Air Temperature, Barometric Pressure, Residuals, Adjusted Residuals, Wind Direction, Wind Gust, Wind Speed.

XGBoost constructs a boosting tree (BT) model which is a type of ensemble model with multiple decision trees to improve predative accuracy of the model (Chang, Chang et al., 2018). The model adds trees to correct the errors caused by the previous trees, then, the process is repeated until a predefined stopping criterion is met. At each time, a weighted set of the training sample is used to train each tree, where the weights are optimised according to the prediction errors of the previous trees (Chang, Chang et al., 2018). XGBoost employs a forward addition policy where each time a decision tree is added by the model. The previous function learns a new function and its coefficients used to fit the residuals of the last step of the prediction.

$$y_m^n = y_m^{n-1} + f_m(x_m) \tag{15}$$

$$obj^m = \sum_{m=1}^{n} L(y_m, y^{n-1}L + f_n(x_m) + \omega(f_m) \tag{16}$$

Where y_m^n denotes to the perdition value of x_m at step time m, L is the loss function that is used to measure the difference between the actual and predicted values, f_m refers to the decision function, ω denotes to the regulation term that optimise the complexity of the model.

XGBoost approximates the objective function using Taylor expansion to second order polynomial function. This can reduce the complexity of XGBoost and improve its performance by employing first and second derivatives of the loss function. The objective function can be modified as

$$obj^m = \sum_{m=1}^{n}\left[L\left(y_m, y^{n-1}\right) + g_m f_n(x_m) + \frac{1}{2}h_m f_m^2(x)\right] + \omega(f_m) \tag{17}$$

Where g_m and $h_m$are the first and second derivatives of L respectively. To minimise repetition, the XGBoost combines the same values of function one the same leaves. For each leaf node, the optimal weight is calculated using Eq. and the objective function is modified as Eq.

$$w_i = \frac{G_i}{H_i + \rho} \tag{18}$$

$$ob^i = -\frac{1}{2}\sum_{i=1}^{R}\frac{G_i}{H_i + \rho} + \gamma R + C \tag{19}$$

w_i denotes to the weight of the j node, the G_i, H_i are the summation of the first and second derivatives of L for all samples on the i level, γ is the complexity of parameters, ρ is the regularisation parameter, and R is the total number of leaves, and C is a constant. The performance of XGBoost is significantly affected by the selection of parameters. Learning rate, max depth which manages the maximum depth of the tree, are considered crucial parameters for the XGBoost (Bentéjac, Csörgo et al., 1911). Choosing them is required critical analysis and evaluation.

3.5. Self-attention LSTM model

The self-attention LSTM (Jing, 2019) is a hybrid deep learning model that integrates the benefits of self-attention techniques with LSTM. The self-attention LSTM has the capability to model both short-term and long-term dependencies in the complex and non-stationary time series through store and update information across time using a memory cell (Cai, Gao et al., 2024). Moreover, the self-attention technique is employed to capture hidden patterns in time series that change over time (Zang, Xu et al., 2021).

The self-attention LSTM model involves two techniques: an LSTM encoder, and a self-attention decoder. The LSTM encoder encodes the received input sequence as a hidden state vector that extracts the information of the input sequence while the self-attention decoder receives the hidden state vector as an input and creates an output vector to represent the prediction of the next value in the sequence. To identify the prediction contribution of each position in the sequence, a query key value technique is included in the self-attention decoder. The query key value technique assigns an attention score for each position the sequence.

The self-attention decoder also produces a context list that includes a weighted sum of the input lists, where the weights are calculated using the attention scores. Then, all context lists are combined along with the hidden state vector, and they are passed through a fully connected layer to generate the output vector. The main formula of the self-attention LSTM is expressed as follows:

Suppose an input time series data $X = \{x_1, x_2, x_3, \ldots., x_k\}$, where $x_i \in \mathbb{R}$ is m-dimensional feature vector at time step t. For each time step t, the LSTM encoder calculates the hidden state vector by the following questions:

$$f_t = \rho\left(w_f x_t + u_f h_{t-1} + b_f\right) \tag{20}$$

$$I_t = \rho(w_I x_t + u_I h_{t-1} + b_I) \tag{21}$$

$$O_t = \rho(w_O x_t + u_O h_{t-1} + b_O) \tag{22}$$

$$c_t = \rho * c_{t-1} + I_t * tamh(w_c x_t + u_c h_{t-1} + b_c) \tag{23}$$

$$h_t = O_t * \tanh(C_t) \tag{24}$$

Where $I_t,\ f_t, O_t$ are the input gate, forget gate, and output get respectively, ρ is the activation function, $*$ refers to the multiplication operator, c_t denotes to the cell state vector, $w,\ u,\ b$ are learnable parameters.

The last hidden layer h_t is sent as an input to self-attention decoder to generate the next prediction value $y_t + 1$. A query key value technique is involved in the self-attention decoder. The query key value technique assigns an attention score for each position the sequence. The attention score is computed using the following formula:

$$e_{mj} = v^T\ tanh\left(w_1 h_j + w_2 h_k + b_1\right) \tag{25}$$

Where $v,\ w_1,\ w_2,\ b_1$ denotes to the learnable variables. All attention scores are normalised using Softmax function to assign attention weight $a_{m,j}$ for each position belong to the input sequence. Where $a_{m,j}$ is calculated using the following equation.

$$a_{m,j} = \frac{\exp\ (e_{mj})}{\sum_{k=1}^{T}(\exp\ (e_{mj}))} \tag{26}$$

Then, a context vectors c_{k+1} is generated by the self-attention layer. The context vectors c_{k+1} is represented by the sum of weight of the hidden state vectors of the input sequence. The context vector is computed by

$$c_{k+1} = \sum_{j=1}^{T} a_{m,j}\ + h_j \tag{27}$$

Then, the context vectors c_{k+1} is accumulated with the last hidden layer and transfer through fully connected layer to form the output vector. The output vector is calculated using the following formula:

$$y_{k+1} = w_3[h_k,\ c_{k+1}] + b_2 \tag{28}$$

The mean squared error (MSE) represents the objective function of the self-attention LSTM. MSE measures the accuracy by calculating the difference between the predicted and actual values of the output sequence. Adam optimizer is employed to optimise he objective.

3.6. Evalution metrics

Suppose the testing set is denoted by $Seelevel_{testing}$ and the $Seelevel\ _{training}$ refers to the number of training set. In this paper, the proposed model is evaluated using several metrics including the Relative percentage error (RPE) (Kim and Kim, 2016), root square error (RSE) (Hodson, 2022), mean absolute error (MAE) (Hodson, 2022), Willmott's index (WI) (Willmott, Robeson et al., 2012), Nash Sutcliffe efficiency (NSE) (McCuen, Knight et al., 2006), Legates and McCabe's (LM) (Legates and McCabe, 2013), and the correlation coefficient (R) (Asuero, Sayago et al., 2006). They are appropriate for sea level prediction as they can capture different characteristics of error, and prediction accuracy such as scale, bias, and variance.

A low value of MAE, RRSE refers to a high performance. While a high value of R means the prediction model delivers accurate predictions and vice versa. All the selected metrics are defined in Eqs. (29–35).

$$MAE = mean\left(\sum_{i\in Seelevel_{testing}} \left|X^i - \overline{Y}^i\right|\right) \tag{29}$$

$$RSE = \sqrt{\frac{\sum_{i\in Sealevel_{test}}\left(X^i - \overline{Y}^i\right)^2}{\sum_{i\in Seelevel_{testing}}\left(X^i - mean(X)\right)^2}} \tag{30}$$

$$R = \frac{1}{\left|Seelevel_{testing}\right|}\sum_{i\in Seelevel_{testing}} \frac{\sum_i\left(X^i - mean(X)\right)\left(X^i - mean\overline{X}\right)}{\sum_i\left(X^i - mean(X)\right)^2\left(\sum_{i=1}^{n}\left(\overline{X}^i - mean\overline{X}\right)\right)^2} \tag{31}$$

$$WI = 1 - \left[\frac{\sum_{i\in SPI_{test}}^{N}\left(\overline{Y}_i - X_i\right)^2}{\sum_{i\in Seelevel_{testing}}^{N}\left(\left|\overline{Y}_i - X_i\right| + \left|\overline{Y}_i - X_i\right|\right)^2}\right]\ where\ 0\ \geq WI\ \leq 1) \tag{32}$$

$$NSE = 1 - \left[\frac{\sum_{i\in Seelevel_{testing}}^{N}\left(\overline{Y}_i - X_i\right)^2}{\sum_{i\in Seelevel_{testing}}^{N}\left(\overline{Y}_i - X_i\right)^2}\right],\ where\ 0\ \geq NSE\ \leq 1 \tag{33}$$

$$LM = 1 - \left[\frac{\sum_{i\in Seelevel_{testing}}^{N}\left|\overline{Y}_i - X_i\right|}{\sum_{i\in Seelevel_{testing}}^{N}\left|\overline{Y}_i - X_i\right|}\right],\ where\ 0\ \geq LM\ \leq 1 \tag{34}$$

$$RPE = \frac{1}{N}\sum_{\in SPI_{test}}^{N}\left|\frac{\overline{X} - X}{X}\right|\text{X100} \tag{35}$$

Where X is the real values and $\overline{Y}$ is the predicted sea level values.

4. Model development

In this section, the evluation metrics are explained as well as the tuning paramters, and modeling details of the proposed CEEMDAN-GAFSF-DBiGRU-OLSSA. The proposed model consists of the following steps.

Phase 1. Correaltion Graph (CG).

The raw timse seires is not suitable for direct use in prediction phase as it has several issues such as misiing points. Data preprocessing technique CG is applied to fill the missing points and eliminate low correlated varaibles. A graph correlation provides a powerful methodology to analysis multivariate time series data and its variables relationships [19]. The proposed correlation graph model exposes complex relationship and dynamic interactions between diverse time-dependent variables. By employing correlation networks, the sea level time series was effectively visualized and analysed to find the strength and direction of relationships among the variables. The proposed graph correlation model identified the strongly connected variables [20].

Consider X is a multivariate time series data $X = \{X_1(t), X_2(t), \ldots, X_p(t)\}, t = 1,2,\ldots,T$, where X_i(t) refers to the i th variable at time t in X, each node is represented by one of time series variables X_i(t) including water temperature, air temperature, Barometric pressure, residuals, adjusted residuals, wind gust, wind direction, and wind speed. To connect each two nodes with an edge, the correlations among variables are calculated. A weight for each edge connected two nodes is assigned to reflect the correlation values, with higher absolute values representing stronger relationships. First, the Pearson correlation matrix is computed:

$$Cor_{i,j} = \frac{\sum_{t=1}^{T}\left(X_i(t) - \overline{X_i}\right)\left(X_j(t) - \overline{X}_j\right)}{\sqrt{\sum_{t=1}^{T}\left(X_i(t) - \overline{X_i}\right)^2\left(X_j(t) - \overline{X}_j\right)^2}} \tag{36}$$

where $Cor_{i,j}$ denotes to the correlation between variables X_i, and X_j, and $\overline{X_i}$ refers to the mean of X_i(t) over the time. The resulted correlation matrix R is represented by a symmetric matrix. The correlation matrix R is employed to construct the correlation network $G = (V, E)$ where V denotes to the X_i variable, then an edge is used to connect any two variables $X_i,\ and\ X_j$ if their absolute correlation $R_{i,j}$ exceeds a predefined threshold ρ. Then, the adjacency matrix A is defined as:

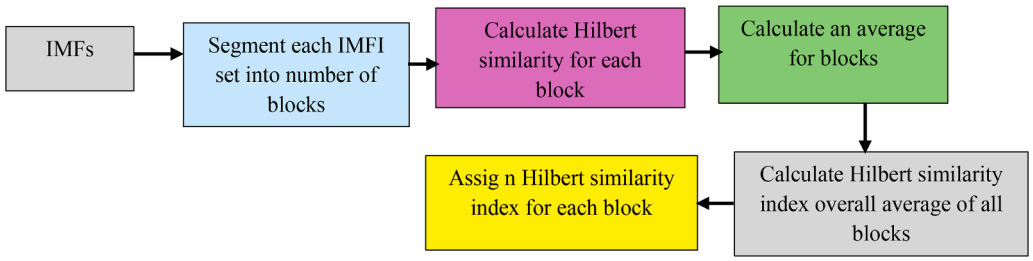

Fig. 3. The architecture of HSF model.

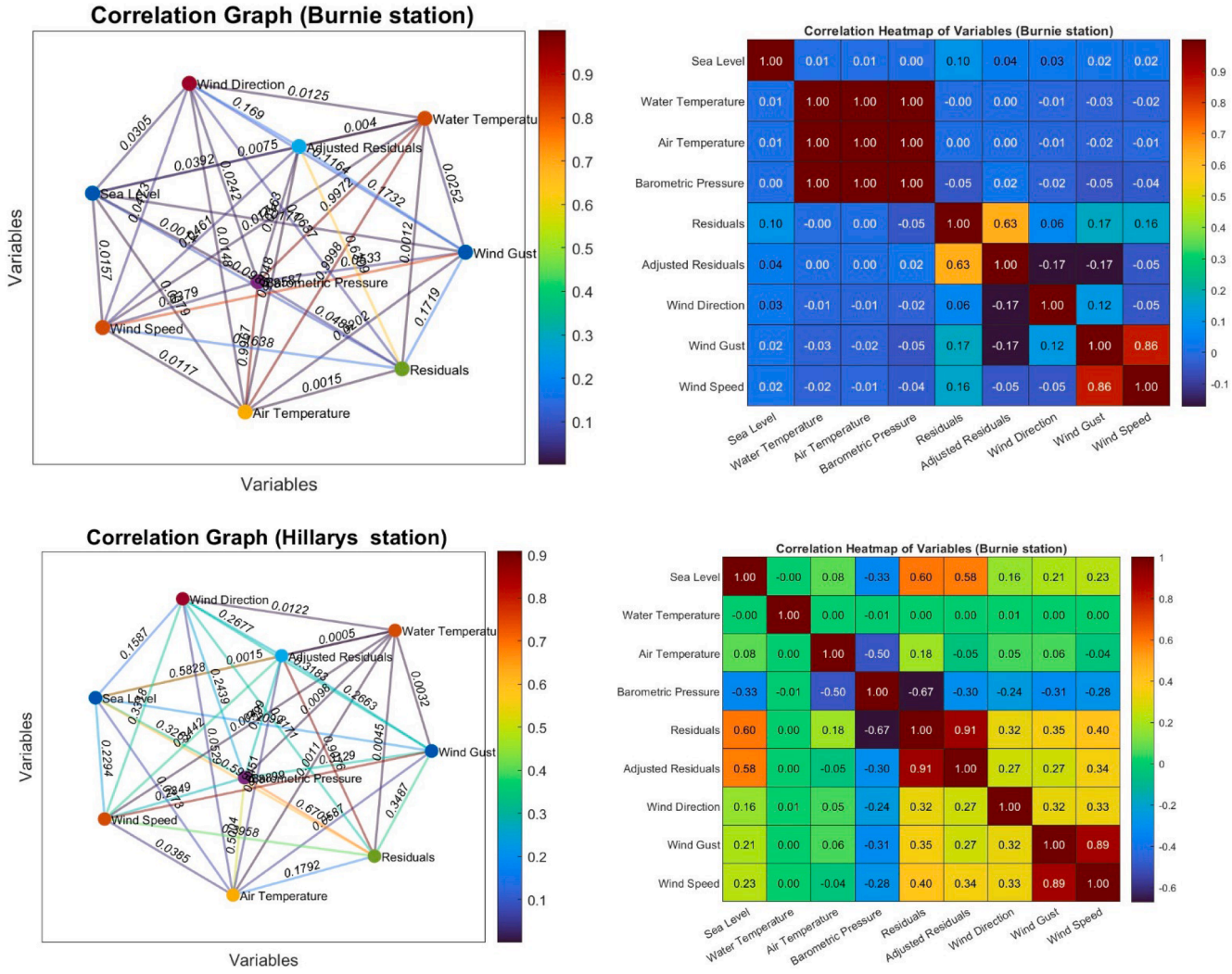

Fig. 4. Correlation graph (CG) and matrix of variables for both Burnie and Hillarys stations.

$$A_{i,j} = \begin{cases} R_{i,j} & if\ |R_{i,j}| \geq \rho \\ 0 & otherwise \end{cases} \tag{37}$$

The threshold ρ is used to eliminate the weak nodes. Fig. 4 display the correlation among sea level data variables. Based on the findings not all variables are highly correlated with sea level rise for example the variable Barometric Pressure is obtained the lowest correlation among the other variables. As a result, in this paper, the variables with high correlation are considered in this research while the other variables are excluded to maintain the model accuracy.

A correlation threshold of $\rho \geq 0.10$ based on the simulation results is adopted, as a result it was found that not all variables correlated equally with the sea level variability. As a results, each variable scored Pearson correlation coefficient below 0.10 was considered weak and it was excluded. Fig. 3 shows the correlation heatmap of all variables. It was noticed that Barometric Pressure recorded the lowest correlation values among the variables and therefore it was excluded.

Although barometric pressure is a known physical driver, its correlation with sea level can vary substantially across regions and time scales depending on local meteorology, coastal geometry, and tidal dominance. In the selected dataset (1999–2024), the inverted barometer influence showed to be masked by stronger drivers such as tidal constituents, wind forcing, and long period oceanic oscillations resulting in a correlation magnitude ($|\rho| \geq 0.10$). Because the study aims to build a data driven prediction model, a correlation based screening step

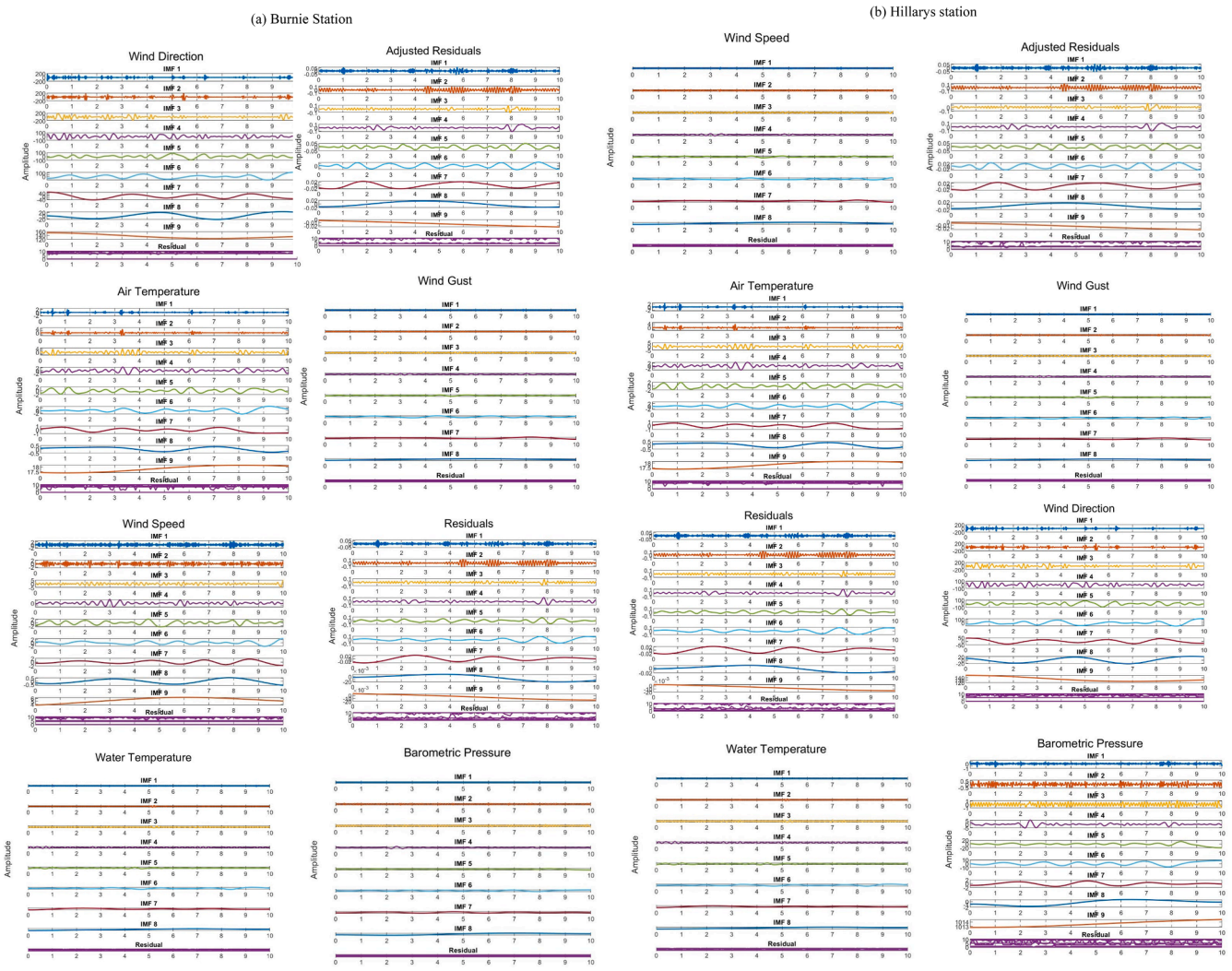

Fig. 5. CEEMDAN based IMFs of input variables for (a) Burnie and (b) Hillarys stations.

is considered to avoid including variables that statistically behaved as noise within this particular station's environment. This does not imply that barometric pressure is universally unimportant, only that within the data available here, its contribution to short-term sea-level variability was negligible.

Phase 2. The CEEMDAN process.

In this phase, CEEMDAN technique is applied to decompose each variable into IMF and resudual components. The target sea level has eight feature. The input varaibles air temperature, adjusted residuals, wind speed, residuals, air temperature, wind direction, and residuals were decomposed into IMFs = 9 while the wind gust, Barometric pressure, and water temperature demarcated into IMFs = 8 for Burnie and Hillarys station. Fig. 5 shows the decomposed IMFs of each variable.

Phase 3. The HSF to select features.

The redundant features could decrease the prediction rate. Therefore, the HSF is designed to extract the optimal feature set to identify the number of IMFs that should be utlised to predict the sea level.

The HFS is selected the IMFs based on the number of features needed (15 %, 20 %, 30 %) and their HFS index is computed using Eq. (12). The output of CEEMDAN consists of several IMFs for each variable, denoted as V1 to Vn, and the block size was set to 3. The HSF index is calculated for each successive blocks, and this process repeated for subsequent blocks. The average HSF index is computed across all variable's partitions. Then, each CEEMDAN mode (i.e., IMF) is evaluated based on the HSF index. The highest HSF index IMFs were selected to predict the sea level while the other is considered useless. Fig. 6 illustrates the selected features based on the HSF in which mean frequency and energy of IMFs are considered as references. The suggested HFS approach offers a computationally effective and scalable solution for high-dimensional time series data analysis.

Phase 4. Designing the Ensemble AEM model.

The framework of the proposed ensemble AEM model is presented in Fig. 7 for sea level forecasting. The proposed ensemble model consists of three phases: models' selection, weight computation, and basic predictor construction. In this paper, the XGBoost, self-attention LSTM, and GRU are used to form the ensemble model. The reason behind the selection of these models is justified in the next section. The AEM is a robust ensemble based adaptive weight calculating is designed and apply to each IMF component separately.

A robust strategy to assign the weight for each model named dynamic weight strategy (DWT) was proposed in terms of ensemble technique to combine the predictions. A pool of models including self-attention LSTM, XGBoost, SVR, GRU, ELM, CNN are used to form the ensemble using the most accurate ones. A weighted average strategy is employed combining the results of the multi-individual based on their prediction error. The ensemble model updates the weights of each individual model at each time step (Lafta, Zhang et al., 2018; Zhang, Li

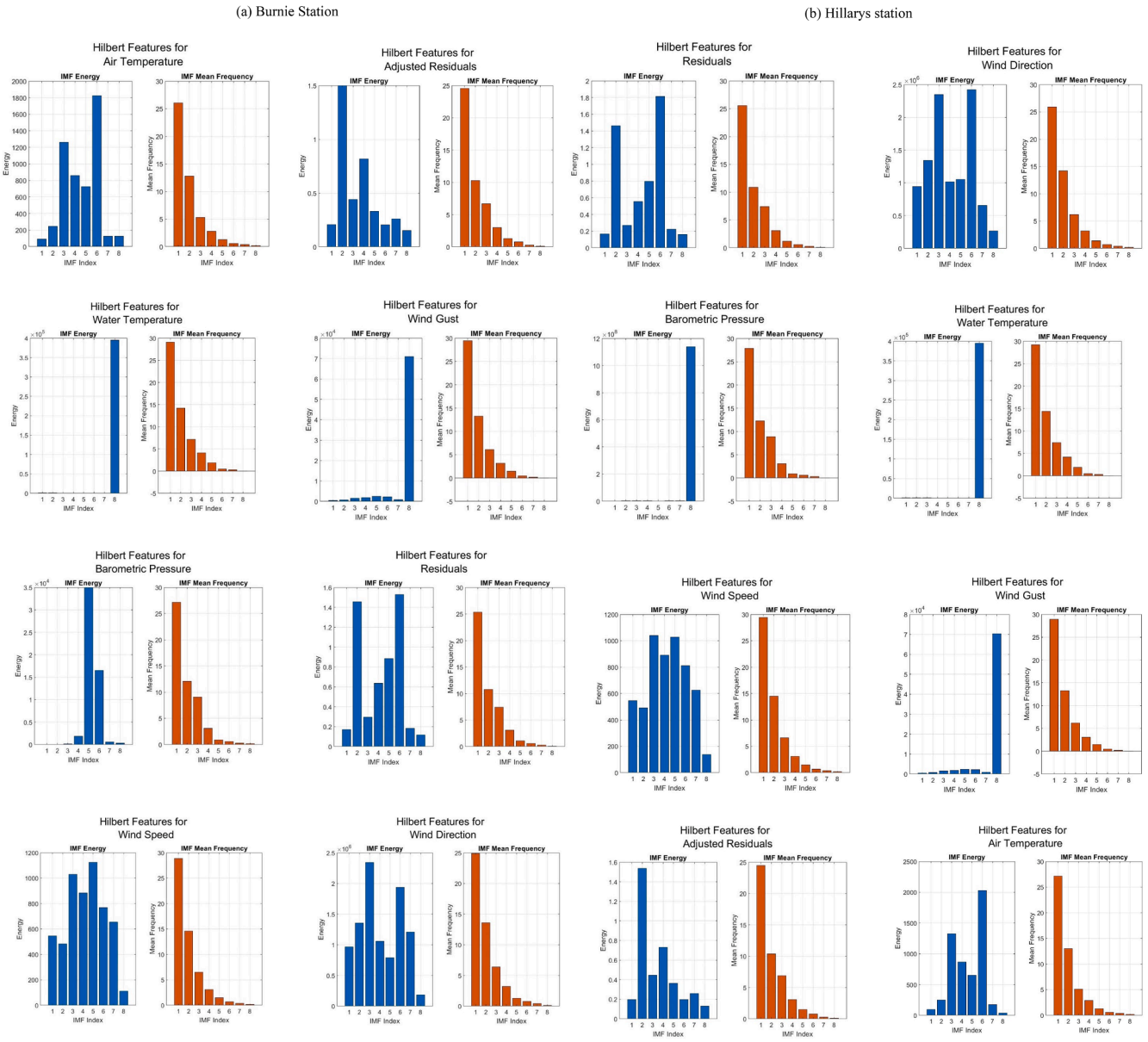

Fig. 6. Histogram of selected IMFs using HFS for (a) Burnie and (b) Hillarys stations.

et al., 2023; Ayinde, Huaming et al., 2024).

Consider a training data at time step t denotes by $D\left\{x_{t,i}, y_{t,i}\right\}$, where $x_{t,i} \in \mathbb{R}$ represents the feature of time series at time step t, and $y_{t,i}$ refers to the actual value of sea level prediction. In addition, there is a pool M of individual models such as *{LSTM, XGBoost, SVR, GRU, Bi-GRU, LightGBM, CNN}* $\{F_m\}_{m=1}^{M}$ that are trained on the same dataset. Each prediction model is denoted by F_m for sample $x_{t,i}$ as $F_m(x_{t,i})$. Also, each model has a memory length of L. Each model uses the previous L of $x_{t,i}$ to predict the $y_{t,i}$. It can be expressed as

$$y_{t,i} = P\left(X_{t-i+1}, \ldots X_{t,i}\right) \tag{38}$$

$$F_m = F_m\left(X_{t-i+1}, \ldots X_{t,i}\right) \tag{39}$$

At each time step, the weight of each model is modified using weighting technique strategy based on their performance and error rate. The weight of each model F_m at time step t as $w_{m,t}$ is computed as follows:

$$w_{m,t} = \frac{\exp\left(-\sigma.error_{m,t}\right)}{\sum_{m=1}^{M}\exp\left(-\sigma.error_{m,t}\right)} \tag{40}$$

Here σ is a hyperparameter used to adjust the sensitivity of weight to error rate, $error_{m,t}$ is the absolute error of each individual model F_m at each time step. The $error_{m,t}$ is defined as

$$error_{m,t} = |Y - F_m(x_t)| \tag{41}$$

The error rate measures the performance of the proposed model. The higher weight obtained by the model results the higher performance. The weight $w_{m,t}$ is updated using the error rate of each model. The weight of each model is calculated for each training sample.

$$error_{m,t} = \frac{1}{k}\sum_{(x,y)\in data(x_t)} |y - F_m(x)| \tag{42}$$

where $data(x_t)$ denotes to the subset sample. The approach extracts the local performance of each model for sample x, and accurate model is obtained a high weight and vice versa. The ensemble model combines

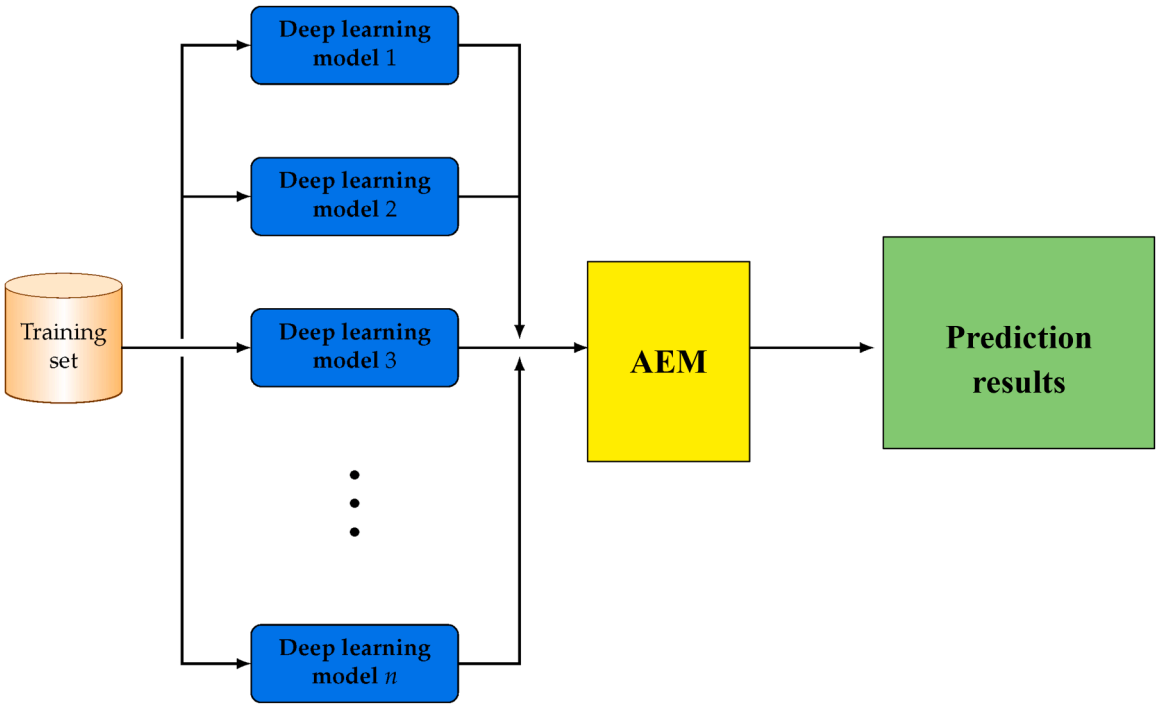

Fig. 7. The proposed AEM model for sea level forecasting.

the predictions of each model. The final prediction result for sample x_t is calculated as follows:

$$F(y) = \sum_{m=1}^{M} w_{m,t} f_m(x_t) \tag{43}$$

The prediction results are expected to be more accurate than individual prediction. Fig. 8 illustrates the schematic view of the proposed sea level forecasting mode

Phase 5. Parameters optimization.

Its important to select carfully the parameters of the AEM models for each IMF. In this paper, oppositional learning sparrow search algorithm (OLSSA) is adopted to select the optimal hyper-parameters to improve its learning ability. For SALSTM, GRU, and XGBoost, the Hidden Units (HU), Dropout Rate (DR), Learning Rate (LR), Attention Heads (AH), Batch Size (BS), Estimators (XGBoost) (ESXGBoost), Max Depth (MDXGBoost), and epoch numbers influence the precision accuracy. As a result, these parameters were the objects of the optimization phase. The final optimization results were reported in Table 1. The proposed model was compared against benchmark models using MATLAB 2024a. The models used in this paper were included ELM, SVR, GRU, SALSTM, XGBoost, and CNN. Table 2 shows the parameters settings of the proposed prediction model and benchmarks models. The proposed model CG-CEEMDAN—HFS-OLSSA was coupled with the ensemble model AEM and all other model ELM, SVR, GRU, SALSTM, XGBoost, and CNN. The parameters of the proposed CG-CEEMDAN—HFS model were listed in Table 2.

4.1. Ensmble construction based on perfromace of different individual models

In this section, the robustness of the proposed CG-CEEMDAN—HFS-OLSSA model is evaluated by creating different combinations of deep learnung models and show the reason behind selection of self-attention LSTM, SVR, XGBoost as ensmble model. In this experiment, time sereis data from 199 to 2024 were selcted for prediction. The seal level data was passed through CG-CEEMDAN—HFS- OLSSA then, the outputs were send to different combination of models as well as individual models. A total of six models including self-attention LSTM (SALSTM), Support Vector Regressor (SVR), XGBoost, Random Forest Regressor (RFR), Gradient Boosting Regressor (GBR), and LightGBM were evaluted. The reason behind selecting thses models as they are more popular and effective in nonstaionary time serie prediction. A different combinationt of enemble were formed from these echniques to evaluate the robustness and dependency of the ensemble model. Each model was traind using pre-processed data to predict the sea level. To choose the best combination of the models, at each time each two models was randomly combined and their performance was recorded using different metrics. Then, the best combination was idenified as an ensemble model for the next round of random model combinations. This process was repeated incrementally to gradually combine more models in the ensemble.

Table 3 report the predition results in terms of MAPE, RMSE, and MAE for each individual model. The results showed that the XGBoost recoreded the lowest MAE and RMSE values, showing the smallest prediction error among the models, while SALSTM scored the lowest MAPE values, demonstrating the highest predictive results among all individul models. The results indicated that the individual models had different limitations and strengths with sea level rise prediction, and combining them may improve the prediction performance.

Tables 4 and 5 report the values of RMSE, MAPE, and MAE for different combination of models. The effecincy of the ensemble model depends on the number and selection of individual model. From the results, some combinations of models scored better predicitive results than the others. The finidng demonstrated that combining more individual models did not essentially enhance performance of the ensmble model. In additiom, when fewer models were integrated, the results becom unstable over different stations. Furthermore, the integration of >4 models could worsen the results compaerd to combination of three models. For example, the combination {SALSTM, XGBoost, GRU, CNN} and {SALSTM, XGBoost, GRU, ELM} scored lower results than {XGBoost, GRU, and SALSTM} although they showed high performnace than all other four combinations.

The best prediction rates were scored by the three combination {XGBoost, GRU, and SALSTM}. The integration of {XGBoost, GRU, and

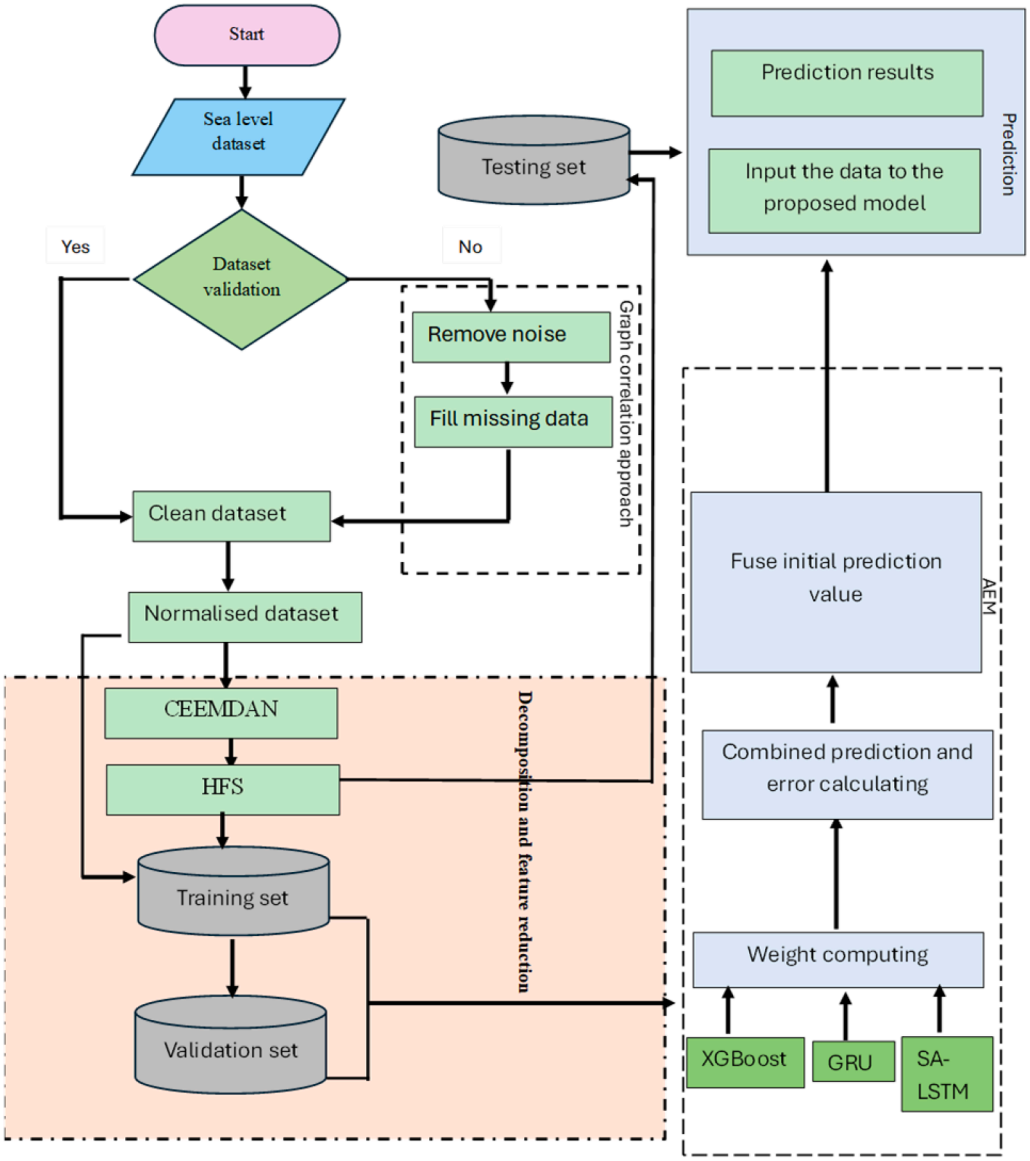

Fig. 8. Schematic diagram of the proposed sea level variability prediction model.

SALSTM} obtained the lowest MAE, RMSE, and MAPE valued. This combination of models showed high capablity in capturing non-linear behaviour and the complex pattrens among veraibles, as well as the spatial dependencies of sea level time seires. The finding showed that the proposed DWT for models integration can modify the weight of IMFs based on the real-time changes in sea level rise. The selected three models including XGBoost, GRU and SALSTM showed a high ability to extract nonlinear relationships in high-dimensional time series as sea level rise which is considered critical factor for accuraet sea level rise prediction. These results in Tables 4 and 5 justified the choice of XGBoost, GRU, and SALSTM to form the esnmbel. They proved to be the most stable, and effective models for sea level rise prediction. The performance of the proposed ensemble model was also compared with the existing esnmble methods.

5. Experimntal results

To avoid data leakage, in this paper, a strictly causal and real time decomposition protocol was applied to ensure that no future information was accessed during the training phase. The time series was chronologically divided into training, validation, and testing sets before applying the decomposition CEEMDAN model, and each set was decomposed independently to prevent temporal cross-contamination. Hilbert spectral features and feature selection were computed solely within the training window and were never fitted on future samples. This strategy mirrors real world prediction, where decomposition was performed sequentially as new data arrive, and ensures that the proposed model learns only from historical observations. The absence of abnormal performance gaps between validation and test sets further confirms that the proposed approach prevents information leakage while maintaining operational prediction realism.

5.1. Results of the self evalution models (Experiment 1)

The proposed model was compared with and without the adaptive ensmeble model (AEM), feature selection (HFS), optimistion method (OLSSA), and correlation graph (CG). More specifically, this experiment compared the CG-CEEMDAN—HSF-AEM with CG-CEEMDAN-AEM, CEEMDAN—HSF-AEM, and CG-CEEMDAN-AEM to demonstrate the efficieny of each model. Furthmore, two other comparison sets were designed with and without OLSSA i.e., CG-CEEMDAN—HSF-AEM-OLSSA vs. CG-CEEMDAN—HSF-AEM to display the benifite of optimsing

Table 1
Paramters for all IMFs of CEEMDAN.

IFM mode	Model	HU	DR	LR	AH	BS	MXXGBoost	ESXGBoost)	epoch
IFM 1	SALSTM	64	0.2	0.001	4	64	-	-	120
	GRU	32	0.2	0.1	-	64	-	-	120
	XGBoost	-		0.001	-	-	120	5	-
IFM 2	SALSTM	64	0.2	0.005	4	64	-	-	120
	GRU	64	0.2	0.005	-	32	-	-	120
	XGBoost	-		0.08	-	-	120	5	-
IFM 3	SALSTM	124	0.2	0.001	4	64	-	-	120
	GRU	64	0.2	0.1	-	32	-	-	120
	XGBoost	-		0.001	-	-	120	5	–
IFM 4	SALSTM	128	0.2	0.005	4	64	-	-	120
	GRU	128	0.2	0.005	-	32	-	-	120
	XGBoost	-		0.08	-	-	120	5	
IFM 5	SALSTM	128	0.2	0.001	4	64	-	-	120
	GRU	128	0.2	0.1	-	32	-	-	120
	XGBoost	-	-	0.001	-	-	120	5	-
IFM 6	SALSTM	128	0.2	0.005	4	64	-	-	120
	GRU	64	0.2	0.005		64	-	-	120
	XGBoost	-	-	0.08	-	-	120	5	-
IFM 7	SALSTM	128	0.2	0.005	4	64	-	-	120
	GRU	128	0.2	0.001	-	64	-	-	120
	XGBoost	-	-	0.07	-	-	120	5	-
IFM 8	SALSTM	128	0.2	0.005	2	64	-	-	120
	GRU	128	0.2	0.001	-	64	-	-	120
	XGBoost	-	-	0.07	-	-	120	5	-
IFM 9	SALSTM	128	0.2	0.005	4	64	-	-	120
	GRU	128	0.2	0.005	-	64	-	-	120
	XGBoost	-	-	0.08	-	-	120	5	-

Table 2
Hyperparmeters the models.

Model	Paramters	Selection approach
ELM	Number of hidden layers=64 and activtion function=Sigmoind	Trail and error
SVR	Kernal=rbf, regulation coffecient =1	Trail and error
GRU	Number of nuron=[12], learning rate=[0.001, 0.01], droupout size=[0.1]	Trail and error
CNN	Learning rate=0.005, kernal size=2.	
The proposed CEEMDAN	CEEMDAN {Signal power thresould=0.05, IMF=10} SALSTM{HU=[128, 64], DR=[0.2], LR=[0.001, 0.005], epoch=120} GRU{HU=[128, 64], DR=[0.2], LR=[0.001, 0.005], epoch=120}	OLSSA

Table 3
Prediction rate for four model for Burnie and Hillarys stations.

Burnie station						
Model	XGBoost	SVR	SALSTM	ELM	GRU	CNN
RMSE	6.657	6.786	7.434	8.564	8.432	8.754
MAE	5.873	5.942	6.343	7.543	7.432	7.754
MAPE	7.234	8.322	8.654	9.433	9.322	9.564
Hillarys station						
RMSE	6.787	6.854	7.532	8.634	8.526	8.806
MAE	5.943	5.998	6.421	7.632	7.543	7.822
MAPE	7.543	8.564	8.732	9.533	9.432	9.734

paramtres. Tables 6 reported the performance of these models in terms of MAE, WI, NSE, LM, RSE, and ACC along with diagnostic visualizations provided in Fig. 9, Fig. 10 and Fig. 11 display using taylor, prediction errors, and regression plots. The details of the forecasting results are described below.

- The effecincy of HSF was assed in this experimrnt by comapring the CG-CEEMDAN—HSF-AEM and CG-CEEMDAN-AEM. According to the results, there were noticable changes in MAPE, RMSE, and MAE and their visualized Taylor plots in Fig. 8. From the obtained results, during the training phase, the perfomnace of the proposed model gradually increased in two station during the period of 2019–2024 when the HSF was applied. The results indicated that the considered HSF model successfully eliminates noisy and redundant features, offering remarkable advantages in improving the perfomnace of CG-CEEMDAN—HSF-AEM model and reducing prediction difficulty.
- From CG-CEEMDAN—HSF-AEM to CEEMDAN—HSF-AEM, evaluting the proposed model with and without the use of correlation graph (CG). As mentioned before, the CG was applied to remove the lower correlated varaibles and keep the higly correlated varaibles to the seal level rise. It can be noticed that the prediction error values of the proposed model in Fig. 8 for both stations were descreased when the CG was invloved. In addition, the vsiual reulst by Taylor, prediction error, and regression confirmed the effecincy of CG.
- With a careful observation of the obtained results in Table 6, and Fig. 8, 9, and 10, it can be noticed that the prediction errors were reduced after including HSF and CG. The proposed CG-CEEMDAN—HSF-AEM model generated a close value to the actual values than CEEMDAN-AEM. This observation in Figs. 8 and 9 using regressions plots demonstrated that the feature selection (HSF) and correlation graph (CG) highly contibuted in improving the predictive accuarcy of the proposed model.
- In this experiment, the benefits of OLSSA was demostrated . The compariosns between CG-CEEMDAN—HSF-AEM-OLSSA and CG-CEEMDAN—HSF-AEM showed that the oprimisation model OLSSA improved the results by 1.5 % and the learning ability of the propsoed model CG-CEEMDAN—HSF-AEM was improved and the model become more accurate to produce very close value to the actual.

5.2. Model comparison with benchmark models (Experiment 2)

The proposed CG-CEEMDAN—HSF-AEM- model was compared with two classes of popular time series prediction models to further examine its generalisttiy and validity. Firslty it was comapred with most popular ensmble models including adaptive weighted average (AWA), voting

Table 4
Performance evaluation for different combination of models for Burnie station.

Model	Combination of two models							
	RSME	MAE	**KGE**	R	**LMI**	NSE	**WI**	APB
SALSTM, XGBoost	**8.423**	**6.462**	**0.851**	**0.831**	**0.822**	**0.813**	**0.823**	**6.330**
SALSTM, SVR	8.525	6.320	0.795	0.793	0.793	0.796	0.792	7.550
CNN, ELM	9.344	8.970	0.756	0.744	0.742	0.732	0.737	7.780
ELM, SALSTM	8.673	6.670	0.784	0.783	0.783	0.788	0.782	7.550
SALSTM, GRU	12.34	11.740	0.754	0.756	0.765	0.72	0.726	7.960
GRU, XGBoost	16.23	14.300	0.714	0.710	0.712	0.705	0.741	8.270
GRU, SALSTM	8.212	6.312	0.876	0.876	0.874	0.872	0.872	5.221
Combination of three models								
SALSTM, XGBoost, SVR	6.231	4.931	0.901	0.902	0.900	0.901	0.899	2.763
SALSTM, XGBoost, CNN	7.67	5.765	0.854	0.853	0.843	0.851	0.850	4.43
SALSTM, XGBoost, GRU	**4.911**	**3.931**	**0.980**	**0.980**	**0.981**	**0.972**	**0.991**	**1.623**
SALSTM, XGBoost, ELM	7.324	6.543	0.853	0.846	0.848	0.843	0.845	5.143
CNN, XGBoost, SVR	8.101	6.212	0.805	0.812	0.802	0.809	0.812	7.250
SVR, GRU, SLM	6.897	5.131	0.876	0.886	0.875	0.883	0.870	2.987
SVR, GRU, CNN	7.874	5.890	0.847	0.844	0.835	0.837	0.844	4.65
SVR, GRU, SALSTM	6.654	5.211	0.886	0.882	0.870	0.872	0.876	2.867
SVR, GRU, XGBoost	7.76	5.54	0.832	0.824	0.821	0.820	0.822	7.12
CNN-GRU-SALSTM	7.411	5.541	0.852	0.851	0.845	0.846	0.842	4.32
Combination of four models								
SALSTM, XGBoost, SVR, CNN	6.541	4.956	0.897	0.890	0.887	0.881	0.876	2.790
SALSTM, XGBoost, GRU, CNN	6.621	4.976	0.886	0.889	0.882	0.874	0.873	2.792
SALSTM, XGBoost, SVR, ELM	6.761	4.987	0.874	0.874	0.865	0.864	0.864	2.797
SALSTM, XGBoost, SVR, GRU	5.211	3.998	0.931	0.932	0.921	0.921	0.920	2.321
SALSTM, XGBoost, ELM, GRU	5.321	4.121	0.911	0.910	0.912	0.913	0.911	2.531
ELM, XGBoost, SVR, CNN	6.431	4.921	0.892	0.893	0.885	0.884	0.878	2.651
XGBoost, SVR, CNN, GRU	6.321	4.843	0.902	0.912	0.902	0.912	0.903	2.654
SALSTM, SVR, GRU, ELM	**5.100**	**3.821**	**0.945**	**0.944**	**0.945**	**0.941**	**0.941**	**2.101**
SALSTM, SVR, CNN, ELM	5.101	3.854	0.941	0.942	0.941	0.939	0.935	2.121

Table 5
Performance evaluation for different combination of models for Hillarys station.

Model	Combination of two models							
	RSME	MAE	**KGE**	R	**LMI**	NSE	**WI**	APB
SALSTM, XGBoost	**8.342**	**6.322**	**0.852**	**0.832**	**0.823**	**0.814**	**0.823**	**6.320**
SALSTM, SVR	8.511	6.310	0.794	0.788	0.797	0.798	0.798	7.541
CNN, ELM	8.721	8.943	0.773	0.771	0.773	0.763	0.763	7.621
ELM, SALSTM	8.665	6.621	0.786	0.788	0.787	0.789	0.789	7.531
SALSTM, GRU	11.31	9.740	0.762	0.761	0.771	0.765	0.763	7.620
GRU, XGBoost	16.11	14.100	0.712	0.712	0.713	0.700	0.745	8.250
GRU, SALSTM	7.912	6.210	0.880	0.878	0.885	0.880	0.881	4.011
Combination of three models								
SALSTM, XGBoost, SVR	6.211	4.921	0.900	0.900	0.901	0.900	0.900	2.761
SALSTM, XGBoost, CNN	7.54	5.711	0.861	0.857	0.856	0.857	0.857	4.410
SALSTM, XGBoost, GRU	**4.910**	**3.930**	**0.986**	**0.985**	**0.985**	**0.974**	**0.995**	**1.621**
SALSTM, XGBoost, ELM	7.311	6.512	0.857	0.848	0.849	0.847	0.848	5.141
CNN, XGBoost, SVR	7.900	6.200	0.812	0.814	0.817	0.818	0.818	6.234
SVR, GRU, SLM	6.893	5.130	0.878	0.888	0.879	0.886	0.875	2.985
SVR, GRU, CNN	7.874	5.890	0.847	0.844	0.835	0.837	0.844	4.650
SVR, GRU, SALSTM	6.611	5.200	0.888	0.889	0.887	0.878	0.879	2.852
SVR, GRU, XGBoost	7.73	5.53	0.836	0.826	0.827	0.827	0.828	6.920
CNN-GRU-SALSTM	7.211	5.512	0.859	0.859	0.846	0.846	0.847	4.30
Combination of four models								
SALSTM, XGBoost, SVR, CNN	6.511	4.921	0.899	0.899	0.889	0.888	0.878	2.770
SALSTM, XGBoost, GRU, CNN	6.611	4.954	0.886	0.890	0.892	0.886	0.883	2.781
SALSTM, XGBoost, SVR, ELM	6.731	4.976	0.877	0.877	0.868	0.869	0.869	2.797
SALSTM, XGBoost, SVR, GRU	5.212	3.999	0.930	0.933	0.923	0.924	0.924	2.320
SALSTM, XGBoost, ELM, GRU	5.320	4.120	0.912	0.912	0.913	0.914	0.914	2.534
ELM, XGBoost, SVR, CNN	6.430	4.920	0.899	0.898	0.888	0.888	0.877	2.650
XGBoost, SVR, CNN, GRU	6.320	4.842	0.901	0.912	0.903	0.914	0.914	2.651
SALSTM, SVR, GRU, ELM	**4.921**	**3.701**	**0.953**	**0.949**	**0.949**	**0.949**	**0.948**	**2.000**
SALSTM, SVR, CNN, ELM	5.000	3.821	0.948	0.949	0.947	0.949	0.941	2.120

regressor (VR), and stacking regressor (SR). Secondly, it was compared with the standard individual models including RF, BiGRU, BiLSTM. Prediction results for each model was detailed in Table 7. Figs. 11, 12, 13 and 14 display the numerical visualizations for the prediction results for each model in Experiment 2.

The results demonstrated that the proposed model significantly improved sea level rise prediction comapred against the benchmarking models, consistently attaining reliable accuracy across the two stations and evaluation metrics. The results in Table 7 from two stations Burnie, and Hillarys stations showed that the proposed model attained the highest WI=0.982, NSE=0.971, LM=0.9721, CC= 0.98, and WI=0.976, NSE=0.98, LM=0.972, CC=0.972 for two stations Hillarys and Burnie,

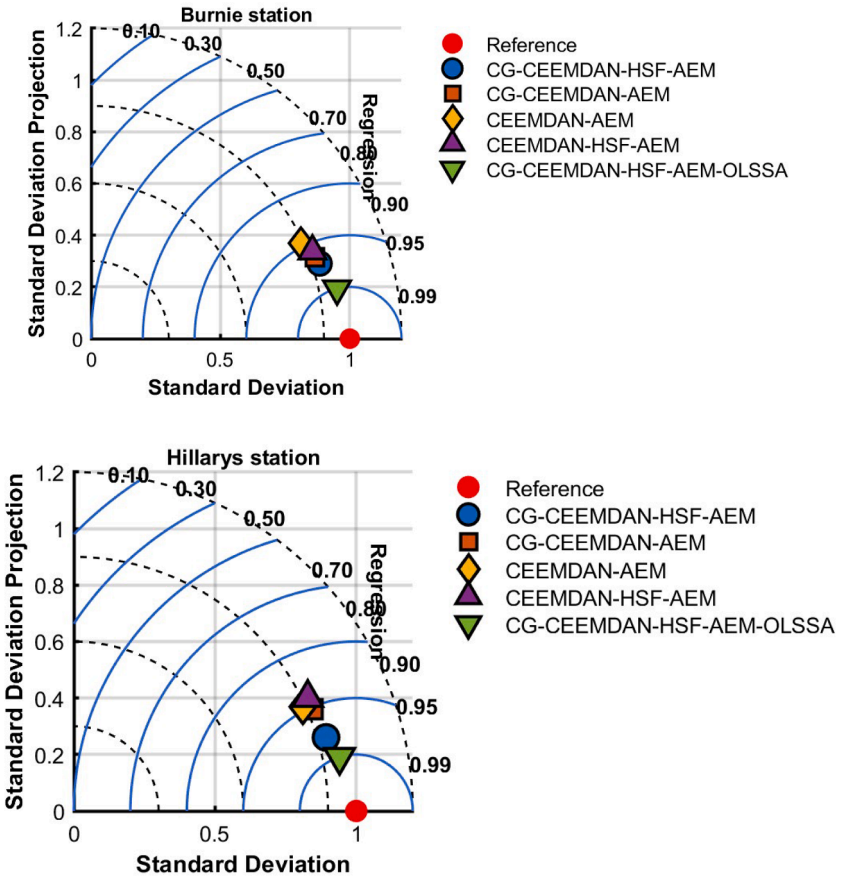

Fig. 9. Taylor plot for two stations for all models.

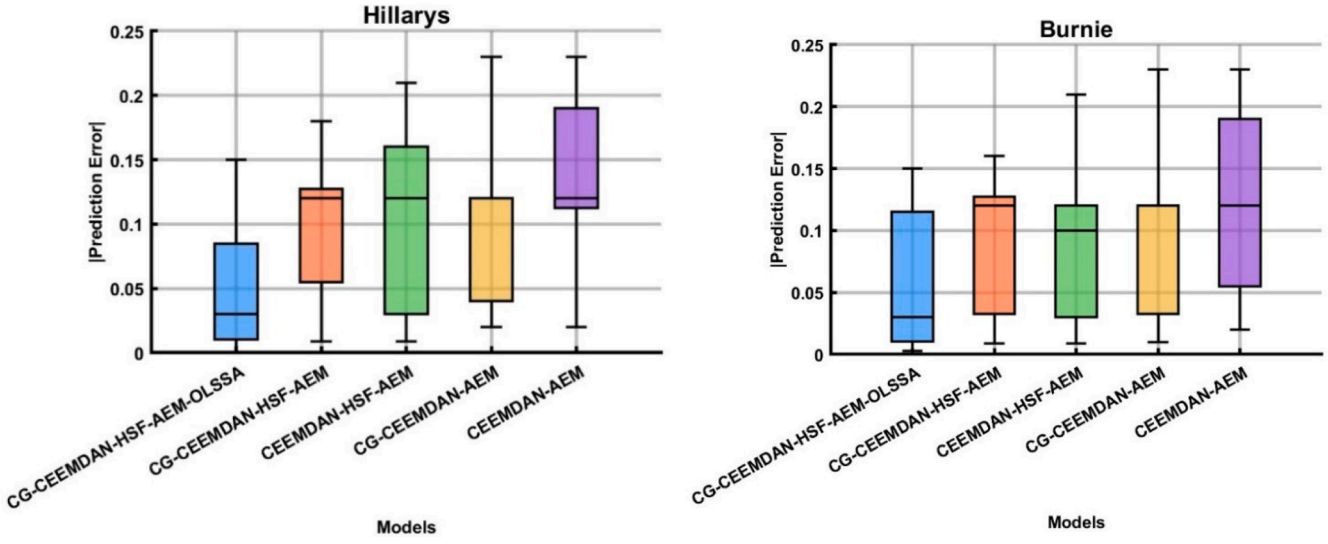

Fig. 10. Prediction error plots for all models.

and the lowest MAE=3.930, RSE=2.12(Hillarys station), MAE=3.941, RSE=2.14 (Burnie station). The scond highest accuracy was scored by AWA model comapred with other models for two stations.

Although traditional ensmble strategy including VR and SR are useful in time series predition, they could fail in capturing the irregulaer behaviour with real time data variability confronted in sea level rise prediction. The proposed ensmble AEM model enabled the CG-CEEMDAN—HSF to adjust more effectively to changing in seal level rise conditions, delivering superior predictive accuracy. Taylor plot and box plots shown in Fig. 12 were also employed to further evalute the proposed model. Based on the results obtained by Taylor plots, it can be noticed that the propsoed model generated very close values to the acual ones for two stations. In addition, the prdiction error in Fig. 13 confirmed the findings in Table 7 in which the proposed model gained the lowerst prediction error among the ensemble models.

Fig. 14 shows the predition sequences for each all models for two

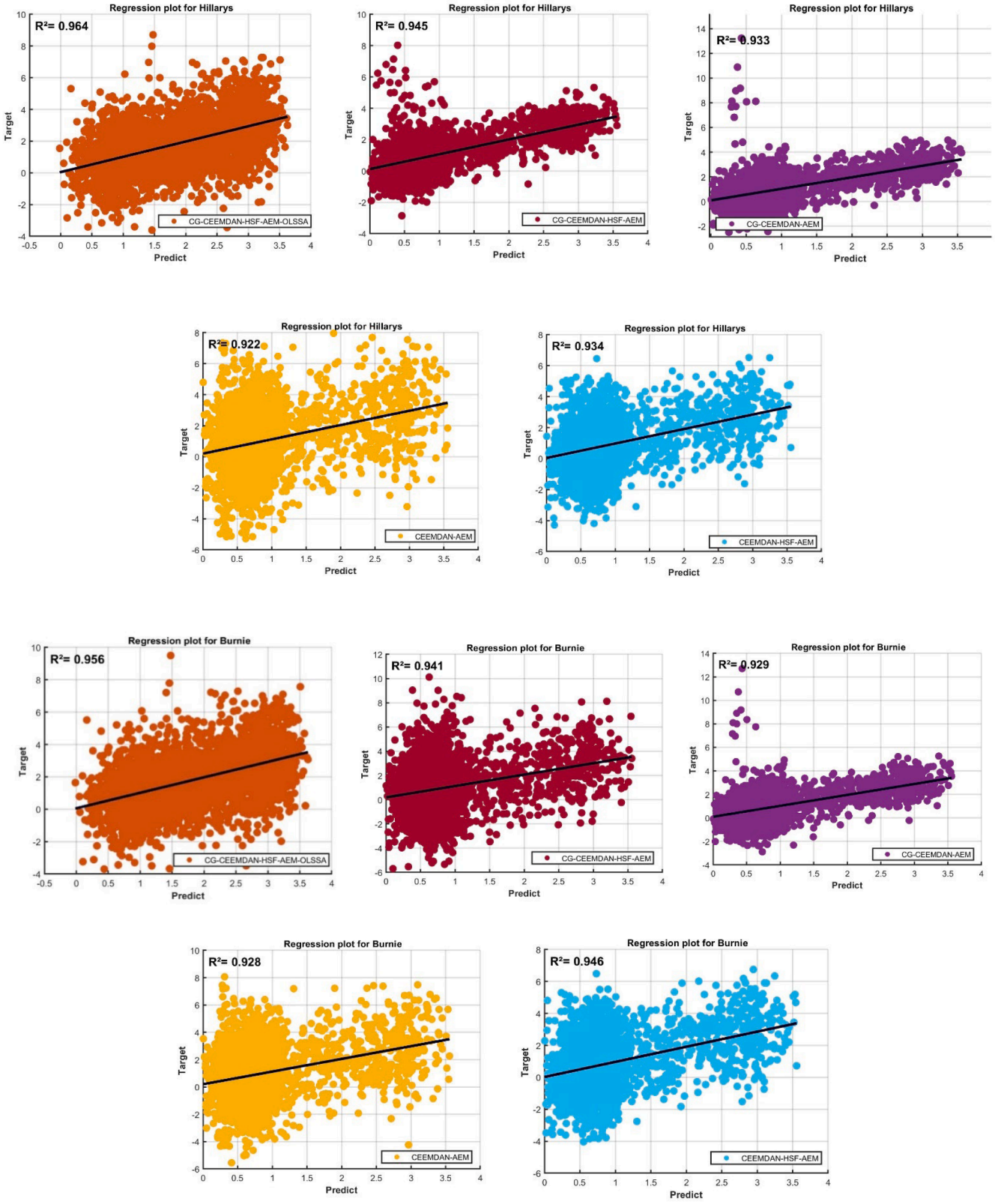

Fig. 11. Regression plot for Hillarys and Burnie stations.

stations. These graphs approved that the propsoed model was contributed signifcanly in reducing epredicition error and increasing the coorlations with the actual values, demonstrating optimal reults by possessing the lowest prediction error, MAE, RSE values for both stations. These findings highlighted that the proposed model CG-CEEMDAN—HSF-AEM better suited to deal with the non-linear relationships and complex pattrens present in sea level rise data. This superiority allows AEM to outperform traditional ensemble approaches in real-time seal level prediction issues, ensuring both efficiency and accuracy.

Table 6
Performance evaluation of the proposed model in Hillarys and Burnie stations.

Hillarys station						
Model	MAE	WI	NSE	LM	RSE	CC
CG-CEEMDAN—HSF-AEM	3.978	0.958	0.960	0.956	2.45	0.966
CG-CEEMDAN-AEM	3.999	0.953	0.945	0.940	2.88	0.943
CEEMDAN-AEM	4.341	0.921	0.920	0.918	3.01	0.912
CEEMDAN—HSF-AEM	4.121	0.933	0.932	0.930	2.89	0.931
CG-CEEMDAN—HSF-AEM-OLSSA	**3.930**	**0.98**	**0.97**	**0.97**	**2.12**	**0.98**
Burnie station						
CG-CEEMDAN—HSF-AEM	3.991	0.943	0.934	0.941	2.63	0.942
CG-CEEMDAN-AEM	4.101	0.942	0.935	0.931	2.92	0.924
CEEMDAN-AEM	4.351	0.920	0.912	0.910	3.32	0.910
CEEMDAN—HSF-AEM	4.124	0.932	0.930	0.921	2.93	0.920
CG-CEEMDAN—HSF-AEM-OLSSA	**3.920**	**0.971**	**0.964**	**0.967**	**2.15**	**0.973**

Table 7
Performance comparisons with ensembles and individual models for Hillarys and Burnie stations.

Hillarys station						
Model	MAE	WI	NSE	LM	RSE	CC
AWA	4.630	0.922	0.91	0.915	4.121	0.910
SR	5.210	0.931	0.93	0.924	4.110	0.920
VR	6.561	0.902	0.93	0.903	4.780	0.900
RF	6.561	0.872	0.873	0.873	5.170	0.872
BIGRU	7.211	0.853	0.843	0.841	5.410	0.845
BiLSTM	6.089	0.885	0.885	0.876	5.501	0.886
CG-CEEMDAN—HSF-AEM-OLSSA	**3.930**	**0.982**	**0.971**	**0.972**	**2.12**	**0.981**
Burnie station						
AWA	4.731	0.921	0.901	0.9102	4.110	0.900
SR	5.100	0.933	0.934	0.927	4.100	0.931
VR	6.523	0.913	0.937	0.921	4.650	0.932
RF	6.532	0.881	0.881	0.880	4.942	0.881
BIGRU	7.232	0.851	0.840	0.831	5.432	0.837
BiLSTM	6.589	0.885	0.884	0.874	5.100	0.865
CG-CEEMDAN—HSF-AEM-OLSSA	**3.941**	**0.976**	**0.972**	**0.973**	**2.14**	**0.967**

5.3. Prediction error variance (Experiment 3)

In this experiment, Prediction error variance (PEV) was employed to the stability and efficeincy of the proposed model. PEV is formultaed by the following formula:

$$PEV = \frac{1}{T}\sum_{n=1}^{T}\left(err_n - \overline{Err}\right)^2$$

Where err_n denotes to the prediction error, and $\overline{Err}$ is the mean prediction error. The prediction model with good stability produces a small *PEV*. Based on the results presnted in Fig. 15, the proposed model scored the lowest *PEV* among all the benchmark models. For the two stations, the proposed model attained 0.132, 0.1023 respectively for Burnie and Hillarys stations. The results revealed that the *PEV* was much smaller which indicated that the stability of the proposed model was much higher than the becnchmarks models proving the superiority of the designed model.

5. Discussion

The proposed CG-CEEMDAN—HFS-AEM model was not used arbitrarily. It was designed precisely to separate and analyse these physically meaningful frequency patterns. High frequency IMFs captured tidal and storm surge oscillations, mid-frequency IMFs reflected atmospheric and wind forcing variability, and low frequency IMFs depicted long term climatic influence. Thus, the decomposition directly corresponds to oceanographic processes, not simply mathematical convenience. In addition, the proposed ensemble model (AEM) was designed to address a fundamental physical challenge. As sea level variability is a non-stationery geophysical process, two base classifiers were employed, first LSTM to capture long range dependencies, and XGBoost to handle non-linear patterns commonly exhibited anomalies. The applied dynamic weighting approach allowed the proposed model to adapt quickly to changes in physical sea conditions and to align with how ocean systems evolve through time.

This section conducted further assessmnet to evalute the proposed model. In addition, main finding and futur work, limitations have been also dissscussed.

1. The proposed model was also evaluted in terms of the index of agreement (IAG) metric . This test was employed to evalute the reliability, and generalizability of the proposed model. The IA was used to measure the percentage of consistency between the predicted and actual values. A higher IAG value refers to a stronger predictive abilty and vers visa. IAG is computed using the following formula.

$$IAG = 1 - \frac{\sum_{i=1}^{m}(Y_i - \overline{Y_i})^2}{\sum_{i=1}^{m}(|Y_i - \widehat{Y}_i| + |\overline{Y_i} - \widehat{Y}_i|)}$$

Where $\overline{Y_i}, Y, \widehat{Y}_i$ refer to the predicted and actual and average of predicted values repectively. The *IAG* values of the proposed model and benchmarks models were pesented in Fig. 16 for the two stations. The results showed that the proposed model scored the largest *IAG* values of approximately 0.982, 0.9712 coressponding to two stations Burnie and Hillarys. From these results, the models were ranked in descending order as daptive weighted average (AWA), voting regressor (VR), and stacking regressor (SR), BiLSTM, BiGRU, and RF. In summary, the proposed model scored the highest values on several evaluation measures, including MAPE, RMSE, MAE, regression, WI, NSE, CC, PEV, and IA comparing with other models, indicating its high reliability, and stablility.

2. The complexity of the proposed model and the convergence ratio were also eximined. In this experiment, each model was executed 5 times, and the average time was considered as a final reference. The execution times for 5 runs and the average for each model were presnted in Table 8. From the obtained reulst, it can observed that the average execution time for the models RF, BiGRU, BiLSTM were shorter than the nesmble models as the ensmeble model invloved multi models and decomposition approach. Each times series sequence was passed through the CEEMDAN algorithm and integrated with feature selection (HFS) and ensemble which consumed more time, however, a significant improvement in prediction accuarcy was achieved. Another obesrvation was found the CG, HSF, and optimasition model contributed in decreasing the model complexity as redundant features and varaibles were eliminated. The RF model had a better comprelxity time than other models. Therefore, the proposed ensemble model AEM made the model more complex, but increased the predidction accuracy.

3. Although the proposed CG-CEEMDAN—HSF-AEM model showed promissing performance, it has certain limitations. First, the optimisation phase requires sevral iterations, which utilises high computational time, resulting in longer prediction times. Second, there are numerous factors influencing sea level rise, and incorporating various influencing factors along with a multi-layer network structure may yield better results. Improvements in these areas warrant further research in the future.

4. Machine learning based approaches have delivered a significant practical fundings for responding and understanding to ongoing oceanic challenges. As global sea level continues to rise due to climate change, it is necessary to design an artificial intelligent model to interpret sea level behaviour. A such model can support decision makers in understanding

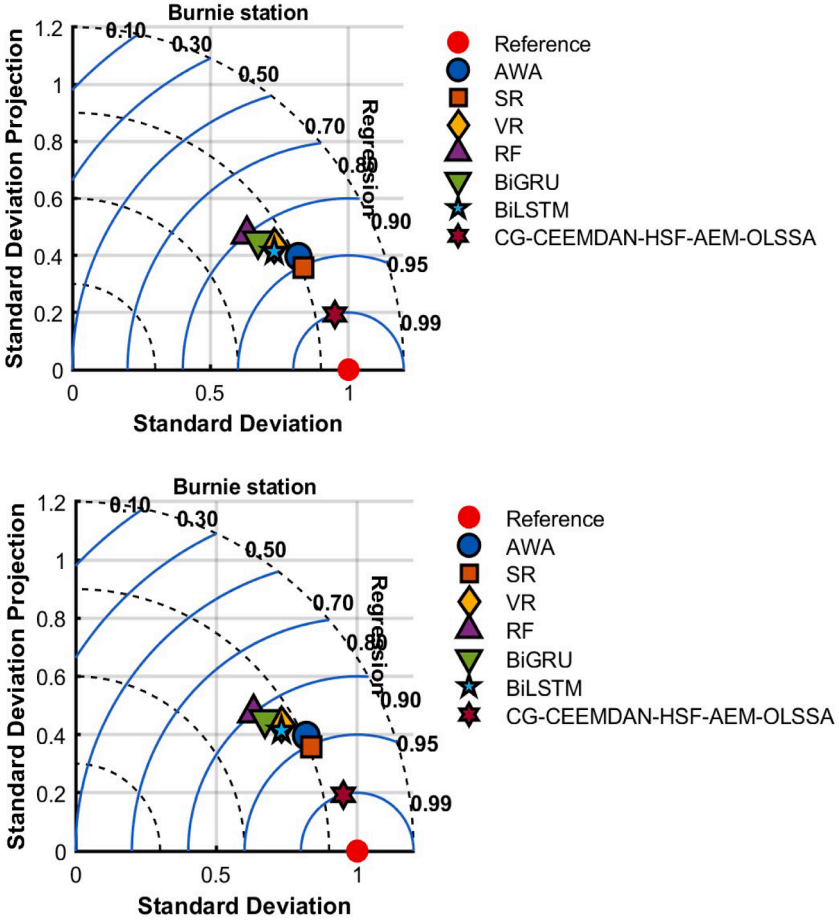

Fig. 12. Taylor plot for two stations for all ensemble models.

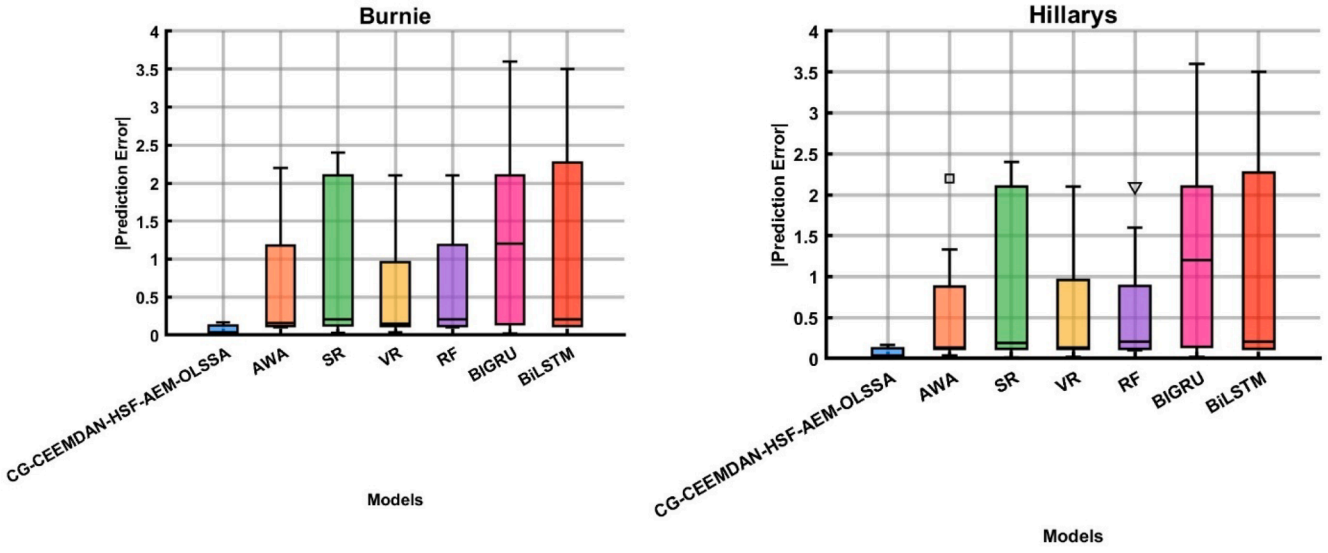

Fig. 13. Prediction error for all ensemble models.

the relationship between sea level rise and coastal erosion. In this paper, CG-CEEMDAN—HFS-AEM-OLSSA model was designed to provide reliable early warning approach for sea level variability. The adopted CEEMDAN model identified dominant oscillatory behaviours associated with climatic drivers, tides, and meteorological patterns. In addition, an adaptive ensemble model was suggested to ensure stable predictions even under non-stationary and rapidly changing conditions. The findings showed that the proposed CG-CEEMDAN—HFS-AEM-OLSSA model was able to extract interpretable patterns that can support experts in understanding the physical mechanisms driving sea level variability. The obtained results highlight the importance of artificial intelligent based approach as practical prediction tools to support climate

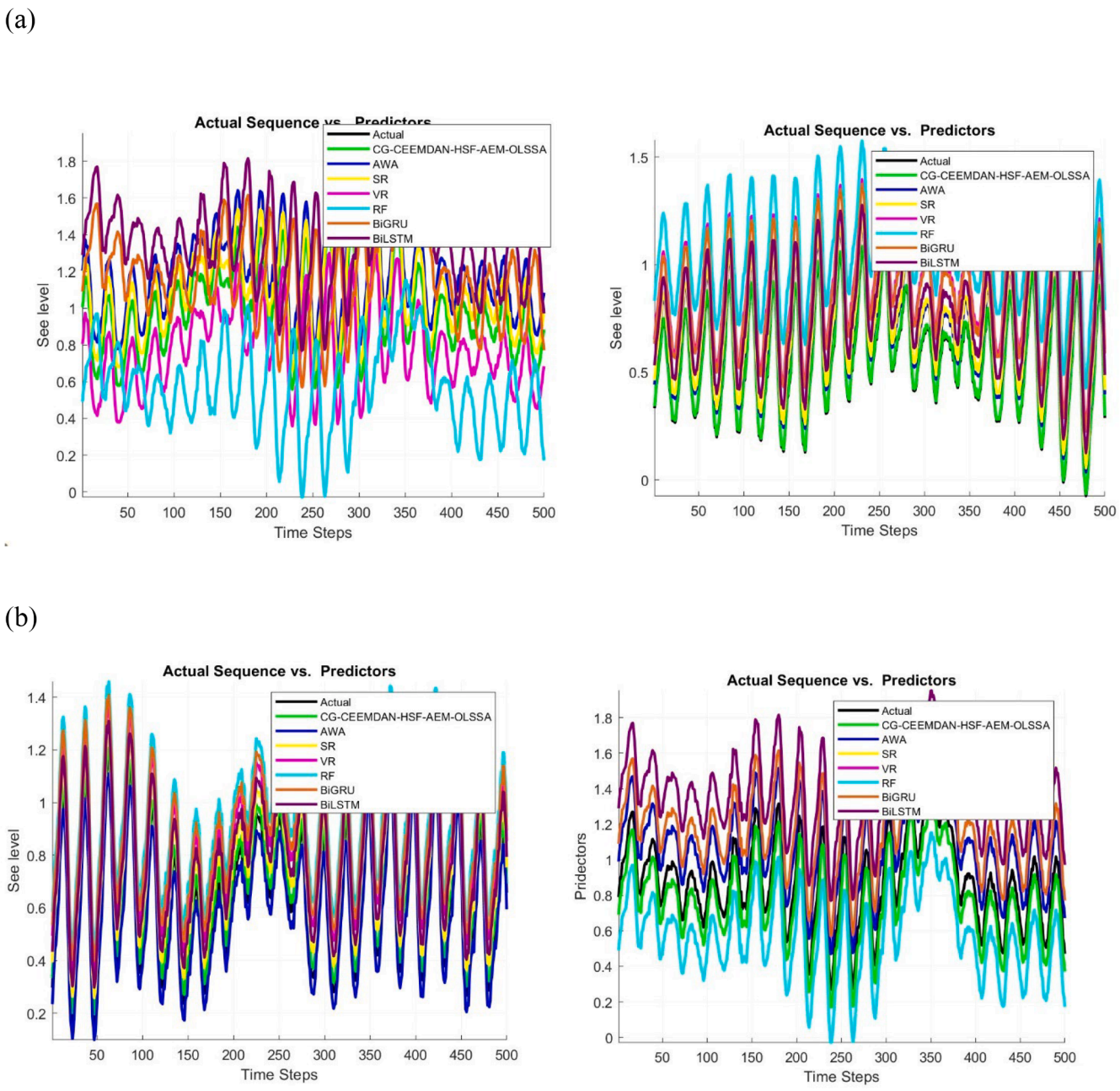

Fig. 14. Sea level trend plots of the models for (a) Burnie and (b) Hillarys stations.

adaptation and resilient coastal-management strategies.

5. Although the proposed CG-CEEMDAN—HFS-AEM model achieved an accurate predictive accuracy, several limitations remain that open pathways for future research. First, the proposed model relied on time series from a limited number of stations, which may limit the model's ability to generalis e across diverse geographic regions with different tidal regimes, climatic drivers, and anthropogenic impacts. Expanding the evaluation to multi continent datasets would strengthen the strength of the proposed model. Second, although the proposed model effectively extracted multi scale and physically meaningful features, the decomposition process was computationally intensive, especially for big time series data and real time applications. Adopting faster real time decomposition or parrel processing strategy would improve scalability. Third, the proposed ensemble model (AEM) updates weights based on error feedback, but it still depended on manually selected base learners; incorporating automated model selection or neural architecture search could further enhance adaptability. Finally, the current study focused on predictive accuracy, but uncertainty quantification critical for decision making in coastal management was not explicitly modelled. Future research should incorporate probabilistic prediction, ensemble uncertainty bands, or Bayesian methods to assess the reliability of predictions. Addressing these limitations will improve the model's practical applicability, computational efficiency, and scientific interpretability.

6. Fig. 17 illustrates the 95 % prediction uncertainty band for the proposed model at two stations. The uncertainty bounds were created from the probabilistic distribution of the absolute prediction errors. Fig. 17 provides a statistically meaningful confidence interval for each prediction sea-level variability. The results indicated that 97.2 % of the observed sea variability measurements fall within the 95 % uncertainty envelope, proving excellent probabilistic consistency between the proposed model and the actual values. The relatively narrow width of the uncertainty band across most tidal cycles showed a low predictive

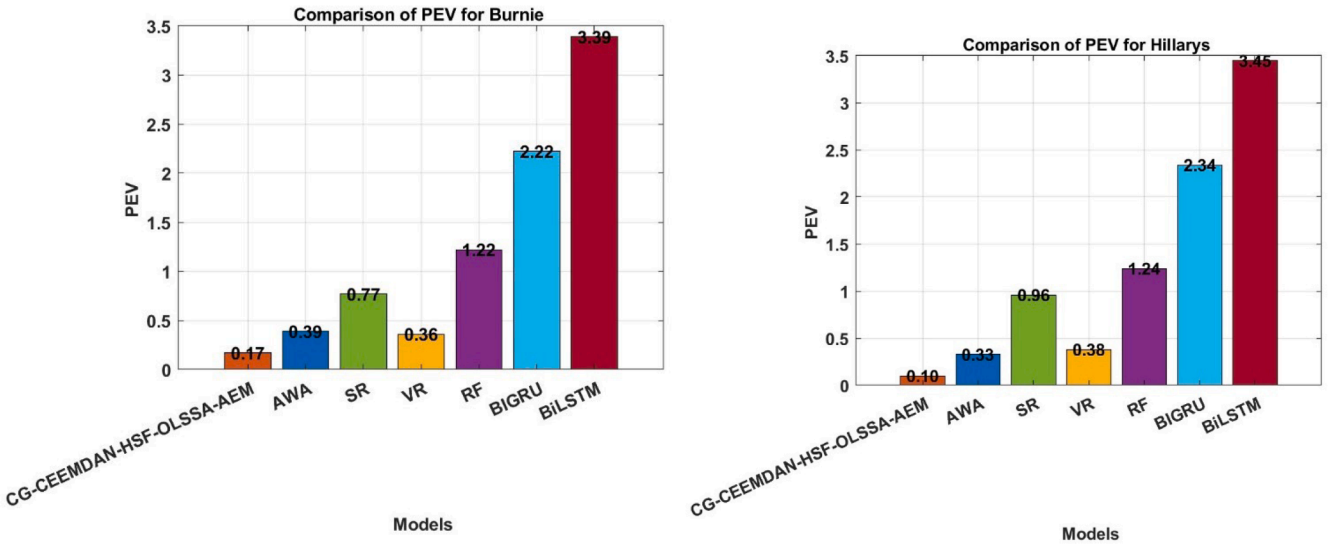

Fig. 15. PEV metric for performance evaluation.

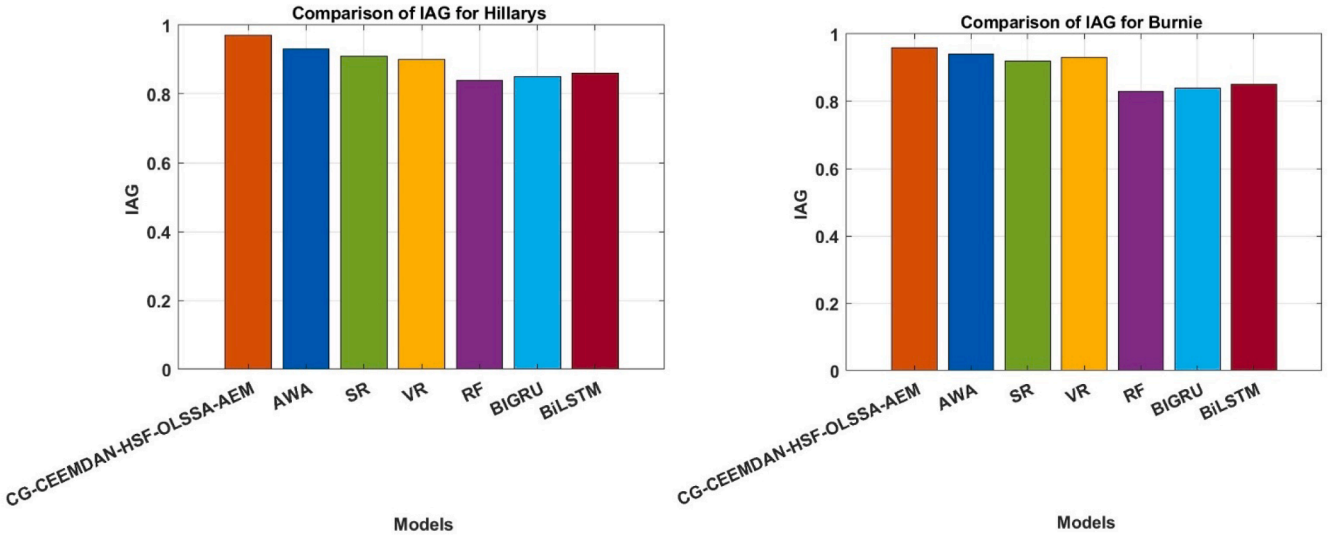

Fig. 16. IAG metric of the model's performance evaluation for each station.

Table 8
Compexity time for 5 runs in milli-second.

Model	Run 1	Run 2	Run 3	Run 4	Run 5	Average
AWA	97.32	96.04	96.21	95.33	95.21	96.21
SR	96.34	94.32	94.03	94.23	94.12	94.54
VR	74.32	73.23	73.09	72.12	73.12	73.11
RF	**14.32**	**13.34**	**13.32**	**13.43**	**12.09**	**12.24**
BIGRU	21.52	22.43	21.45	20.56	20.65	21.1
BiLSTM	24.32	24.21	23.43	23.10	20.21	23.01
CG-CEEMDAN- AEM-OLSSA	112.12	111.23	111.43	111.30	111.16	111.43
CEEMDAN—HSF-AEM-OLSSA	110.21	110.11	109.32	109.32	109.12	`110.12
CG-CEEMDAN—HSF- AEM-OLSSA	102.21	101.43	101.54	101.31	101.87	101.53
CEEMDAN-AEM	125.12	126.21	127.21	126.32	`127.43	126.76

dispersion and high model strength. From a policy perspective, this means that coastal managers can interpret the predicted sea level fluctuations at Hillarys, Burnie stations with a high degree of confidence, since the associated uncertainty was explicitly quantified and tightly constrained.

6. Conclusions

This research work was dedicated to improve the sea level rise prediction through desiging CG-CEEMDAN- HFS-AEM-OLSSA model. The proposed model perfectly integrates graph correlation for preprocessing, decomposition technique (CEEMDAN), novel data feature

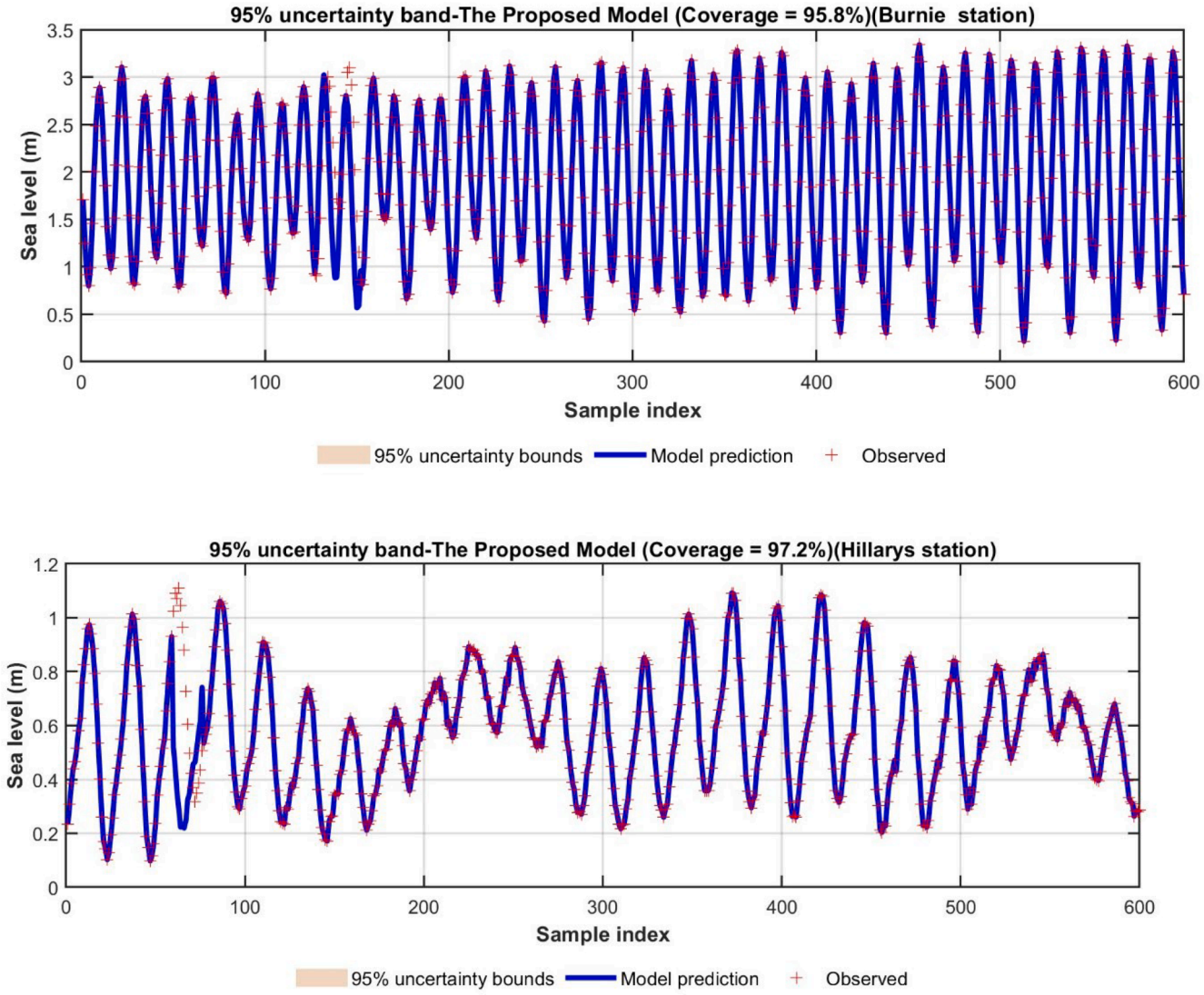

Fig. 17. Probabilistic Uncertainty Bounds (95 %) for the Proposed Sea variability Forecasting Model.

selection (HFS), and robust adpative ensmble model AEM with optimisation algorithm (OLSSA). The ensemble AEM model combines GRU, self-attention LSTM and XGBoost models using dynamic weights assignment strategy, adjusting to real-time changes in sea level rise by updating the weights according to the error and performance of the models. First, the CG removes the lower correlated inputs and fill the missing values. Then the CEEMDAN technique is employed to decompose the CG based inputs into IMFs, followed by HFS to select the most efficient features. The selected features were then used into the AEM model to predict the sea level rise where the OLSSA is adopted as an optimization algorithm to determine the optimal hyper-parameters. To verify the efficiency of the proposed CG-CEEMDAN—HFS-AEM model, experiment 1 was based on the results of the self-evaluation whereas experiment 2 was conducted to compare with different benchmark models to forecast sea level rise for Hillary and Burnie stations in Australia.

The results in experiment 1 demonstrated the ability of the proposed model to successfully remove the redundant features. The outstanding combination of CG-CEEMDAN—HFS proved its ability to improve the prediction accuracy. Moreover, the experiment 3 was designed to prove the abilty of the ensemble adaptive model AEM compared with standard ensemble models. The designed AEM model achieved a remarkable victory in comparison with standard ensemble models, which was evaluted using visual plots and metrics. The proposed model improved accuracy through handling non-linear relationships and capturing complex data patterns, and the potential for real-time, regional-specific predictions of sea level to support the risk management asscoaited with climat changes. Additionally, the proposed model can be used to assess the vulnerability of coastal areas to inundation from sea level rise, and can inform the design and implementation of climate-resilient infrastructure in coastal areas.

CRediT authorship contribution statement

Mohammed Diykh: Writing – review & editing, Writing – original draft, Visualization, Validation, Software, Methodology, Investigation, Formal analysis, Conceptualization. **Mumtaz Ali:** Writing – review & editing, Writing – original draft, Supervision, Methodology, Investigation, Data curation, Conceptualization. **Aitazaz Ahsan Farooque:** Writing – review & editing, Writing – original draft, Supervision, Methodology, Investigation, Conceptualization. **Anwar Ali Aldhafeeri:** Writing – review & editing, Writing – original draft, Supervision, Methodology, Investigation, Conceptualization. **Abdulhaleem H. Labban:** Writing – review & editing, Methodology, Investigation, Conceptualization.

Declaration of competing interest

The authors declare that they have no known competing financial interests or personal relationships that could have appeared to influence the work reported in this paper.

Acknowledgement

This work was supported by the Deanship of Scientific Research, Vice Presidency for Graduate Studies and Scientific Research, King Faisal University, Saudi Arabia [Project No. KFU260104]. The authors would also like to acknowledge the Bureau of Meteorology, Australia for supply the data.

References

Aksoy, M.M., Mowla, M.N., Bilgili, M., Pinar, E., Durhasan, T., Asadi, D., 2025. Forecasting near-surface air temperature via SARIMA and LSTM: a regional time-series study. J. Atmos. Sol.-Terr. Phys., 106604

Ali, Z.A., Abduljabbar, Z.H., Tahir, H.A., Sallow, A.B., Almufti, S.M., 2023. eXtreme gradient boosting algorithm with machine learning: a review. Acad. J. Nawroz Univ. 12 (2), 320–334.

Alshouny, A., Elnabwy, M.T., Kaloop, M.R., Baik, A., Miky, Y., 2022. An integrated framework for improving sea level variation prediction based on the integration Wavelet-Artificial Intelligence approaches. Environ. Model. Softw. 152, 105399.

Altunkaynak, A., Kartal, E., 2021. Transfer sea level learning in the Bosphorus Strait by wavelet based machine learning methods. Ocean Eng. 233, 109116.

Asuero, A.G., Sayago, A., González, A., 2006. The correlation coefficient: an overview. Crit. Rev. Anal. Chem. 36 (1), 41–59.

Ayinde, A.S., Huaming, Y., Kejian, W., 2024. Review of machine learning methods for sea level change modeling and prediction. Sci. Total Environ. 954, 176410.

Bentéjac, C., A. Csörgo and G. Martínez-Muñoz (1911). "A comparative analysis of xgboost." ArXiv abs 392.

Cai, S., Gao, H., Zhang, J., Peng, M., 2024. A self-attention-LSTM method for dam deformation prediction based on CEEMDAN optimization. Appl. Soft. Comput. 159, 111615.

Chang, Y.-C., Chang, K.-H., Wu, G.-J., 2018. Application of eXtreme gradient boosting trees in the construction of credit risk assessment models for financial institutions. Appl. Soft. Comput. 73, 914–920.

Chen, T., T. He, M. Benesty, V. Khotilovich, Y. Tang, H. Cho, K. Chen, R. Mitchell, I. Cano and T. Zhou (2015). "Xgboost: extreme gradient boosting." R package version 0.4-2 **1** (4): 1–4.

Du, C., Xia, M., Peng, X., Guo, H., 2021. Detection algorithm for magnetic dipole target based on CEEMDAN and pattern recognition. Procedia Comput. Sci. 183, 669–676.

El-Diasty, M., Al-Harbi, S., Pagiatakis, S., 2018. Hybrid harmonic analysis and wavelet network model for sea water level prediction. Appl. Ocean Res. 70, 14–21.

Ghorbani, M.A., Khatibi, R., Aytek, A., Makarynskyy, O., Shiri, J., 2010. Sea water level forecasting using genetic programming and comparing the performance with artificial neural networks. Comput. Geosci. 36 (5), 620–627.

Givehki, M., Melby, J., Moreno, F.G., Hodgens, K., Farhadzadeh, A., 2025. Effects of design parameters and sea level rise on lifecycle performance of rubble-mound breakwaters: a computational-statistical framework. Coast. Eng., 104897

Hodson, T.O., 2022. Root mean square error (RMSE) or mean absolute error (MAE): when to use them or not. Geosci. Model Dev. Discuss. 2022, 1–10.

Hsieh, C.-M., Chou, D., Hsu, T.-W., 2022. Using modified harmonic analysis to estimate the trend of sea-level rise around Taiwan. Sustainability 14 (12), 7291.

Imani, M., Kao, H.-C., Lan, W.-H., Kuo, C.-Y., 2018. Daily sea level prediction at Chiayi coast, Taiwan using extreme learning machine and relevance vector machine. Glob. Planet Change 161, 211–221.

Jing, R., 2019. A self-attention based LSTM network for text classification. J. Phys.: Confer. Series. IOP Publishing.

Karimi, S., Kisi, O., Shiri, J., Makarynskyy, O., 2013. Neuro-fuzzy and neural network techniques for forecasting sea level in Darwin Harbor, Australia. Comput. Geosci. 52, 50–59.

Kim, S., Kim, H., 2016. A new metric of absolute percentage error for intermittent demand forecasts. Int. J. Forecast 32 (3), 669–679.

Kowalewski, M., Kowalewska-Kalkowska, H., 2017. Sensitivity of the Baltic Sea level prediction to spatial model resolution. J. Mar. Syst. 173, 101–113.

Lafta, R., Zhang, J., Tao, X., Li, Y., Diykh, M., Lin, J.C.-W., 2018. A structural graph-coupled advanced machine learning ensemble model for disease risk prediction in a telehealthcare environment. Big Data in Engineering Applications. Springer, pp. 363–384.

Lai, V., Ahmed, A., Malek, M., 2019. Modeling the nonlinearity of Sea level oscillations in the Malaysian Coastal Areas using machine learning algorithms. Sustain.

Latif, S.D., Almubaidin, M.A., Shen, C.G., Sapitang, M., Birima, A.H., Ahmed, A.N., Sherif, M., El-Shafie, A., 2024. Improving sea level prediction in coastal areas using machine learning techniques. Ain. Shams. Eng. J. 15 (9), 102916.

Legates, D.R., McCabe, G.J., 2013. A refined index of model performance: a rejoinder. Int. J. Climatol. 33 (4), 1053–1056.

Li, X., Zhou, S., Wang, F., 2025. A CNN-BiGRU sea level height prediction model combined with bayesian optimization algorithm. Ocean Eng. 315, 119849.

Liang, S., Hu, W., Wu, P., Wang, J., Su, S., Chen, G., Du, J., Liu, W., Chen, B., 2023. Prediction of the joint impacts of sea level rise and land development on distribution patterns of mangrove communities. For. Ecosyst. 10, 100100.

Majumder, S., Abeer, A.N., Rahman, M., Bhuiyan, M.A.E., 2025. Analysis and prediction of sea level rise along the US East and Gulf coasts and its socio-economic impacts on the nearby inland areas. Evol. Earth 3, 100051.

Makarynska, D., Makarynskyy, O., 2008. Predicting sea-level variations at the Cocos (Keeling) Islands with artificial neural networks. Comput. Geosci. 34 (12), 1910–1917.

McCuen, R.H., Knight, Z., Cutter, A.G., 2006. Evaluation of the Nash–Sutcliffe efficiency index. J. Hydrol. Eng. 11 (6), 597–602.

Mittal, A., Sachdeva, N., Agrawal, S., Agarwal, S., Kar, P., Varma, M., 2021. Eclare: extreme classification with label graph correlations. In: Proceedings of the Web Conference, p. 2021.

Parker, A., Ollier, C.D., 2017. California sea level rise: evidence based forecasts vs. model predictions. Ocean Coast Manag. 149, 198–209.

Pashova, L., Popova, S., 2011. Daily sea level forecast at tide gauge Burgas, Bulgaria using artificial neural networks. J. Sea Res. 66 (2), 154–161.

Pedronette, D.C.G., Torres, R.D.S., 2016. A correlation graph approach for unsupervised manifold learning in image retrieval tasks. Neurocomputing 208, 66–79.

Qi, L., Lin, W., Zhang, X., Dou, W., Xu, X., Chen, J., 2022. A correlation graph based approach for personalized and compatible web apis recommendation in mobile app development. IEEE Trans. Knowl. Data Eng. 35 (6), 5444–5457.

Willmott, C.J., Robeson, S.M., Matsuura, K., 2012. A refined index of model performance. Int. J. Climatol. 32 (13), 2088–2094.

Xiao, Y., Wu, S., He, C., Hu, Y., Yi, M., 2024. An effective hybrid wind power forecasting model based on" decomposition-reconstruction-ensemble" strategy and wind resource matching. Sustain. Energy Grids Netw. 38, 101293.

Xu, M., Matsushima, H., Zhong, X., Hirabuki, Y., Oka, K., Okoshi, H., Ueno, H., 2024. Prediction of the impact of sea level rise in coastal areas where the tide embankments have been constructed. Landsc. Urban Plan. 252, 105193.

Zang, H., Xu, R., Cheng, L., Ding, T., Liu, L., Wei, Z., Sun, G., 2021. Residential load forecasting based on LSTM fusing self-attention mechanism with pooling. Energy 229, 120682.

Zeiler, A., Faltermeier, R., Keck, I.R., Tomé, A.M., Puntonet, C.G., Lang, E.W., 2010. Empirical mode decomposition-an introduction. In: The 2010 international joint conference on neural networks (IJCNN). IEEE.

Zhang, F., Li, N., Li, L., Wang, S., Du, C., 2023. A local semi-supervised ensemble learning strategy for the data-driven soft sensor of the power prediction in wind power generation. Fuel 333, 126435.

Zhang, H., Cui, N., Yang, K., Qiu, Q., Zheng, J., Li, C., 2025. A comparative evaluation of harmonic analysis and neural networks for Sea level prediction in the Northern South China Sea. Sustainability 17 (13), 6081.

Zhao, J., Cai, R., Sun, W., 2021. Regional sea level changes prediction integrated with singular spectrum analysis and long-short-term memory network. Adv. Space Res. 68 (11), 4534–4543.

Wang, Q., Bai, J., Li, Y., Xiang, S., Chu, X., Sun, Y., Zhang, T., 2025. Sea Level anomaly prediction with TSTA-enhanced UNet. ISPRS J. Photogramm. Remote Sens. 229, 382–395.